Vestnik KRAUNC. Fiz.-Mat. Nauki. 2026. vol. 54. no. 2. P. 166 - 200. ISSN 2079-6641

PHYSICS

https://doi.org/10.26117/2079-6641-2026-54-2-166-200

Review Article

Full text in English

MSC 86A10

PACS 52.80.Mg, 92.60.Pw

Dedicated to the 85th anniversary of Professor P.P. Firstov

Electric Activity of Volcanic Clouds and Formation of Local Electric Field in Kamchatka

E. I. Malkin*, N. V. Cherneva

Institute of Cosmophysical Research and Radio Wave Propagation FEB RAS,
684034, Paratunka, Elizovo raion, Kamchakskiy kray, Russia

Abstract. The paper summarizes the contribution of Firstov P.P. to experimental studies of the vertical component of the atmospheric electric field (AEF E_z) at Paratunka Observatory (2006–2018). Based on the analysis of 47 publications and a monograph (Cherneva and Firstov, 2018), the key role of seasonal radon outflow in the formation of E_z variations is demonstrated. The basic models of field sources are presented, including the influence of steam-water clouds, cyclones, and volcanic eruptions. In particular, a laboratory experiment with the injection of a steam-water mixture from a geothermal well, simulating the impact of an artificial cloud on the AEF E_z, is described. Examples of the influence of cyclonic activity and eruptive clouds from explosive volcanic eruptions on the AEF E_z are given. Firstov P.P. was interested in this topic because of the region specific features, high intensity of geodynamic processes in the Kuril-Kamchatka subduction zone (frequent earthquakes and volcanic eruptions) and sudden variability of meteorological parameters due to intense cyclonic activity over the north-western Pacific Ocean. Particular attention is given to Firstov's initiative to deploy a volcanic thunderstorm recording network in Kamchatka. Using the WWLLN data, the two-stage mechanism for volcanic thunderstorm development was empirically confirmed, and the proposed method for assessing the eruption intensity based on pulsed electromagnetic radiation (PEMR) counting rate is recommended as an early warning tool for ash emissions.

Key words: atmospherics registration, direction, electromagnetic pulses, VLF direction finder, lightning, atmospheric electric field.

Received: 23.07.2026; Revised: 31.08.2026; Accepted: 01.09.2026; First online: 14.09.2026

For citation. Malkin E. I., Cherneva N. V. Electric activity of volcanic clouds and formation of local electric field in Kamchatka. *Vestnik KRAUNC. Fiz.-mat. nauki.* 2026, **54**: 2, 166-200. EDN: RLPGRY. https://doi.org/10.26117/2079-6641-2026-54-2-166-200.

Funding. The work was supported by IKIR FEB RAS State Task (Reg. No. NIOKTR 124012300245-2)

Competing interests. There are no conflicts of interest regarding authorship and publication.

Contribution and Responsibility. All authors contributed to this article. Authors are solely responsible for providing the final version of the article in print. The final version of the manuscript was approved by all authors.

***Correspondence:** E-mail: malkin@ikir.ru

The content is published under the terms of the Creative Commons Attribution 4.0 International License

© Malkin E. I., Cherneva N. V., 2026

© Institute of Cosmophysical Research and Radio Wave Propagation, 2026 (original layout, design, compilation)

Вестник КРАУНЦ. Физ.-мат. науки. 2026. Т. 54. №2. C. 166 - 200. ISSN 2079-6641

ФИЗИКА

https://doi.org/10.26117/2079-6641-2026-54-2-166-200

Обзорная статья

Полный текст на английском языке

УДК 551.594.6

Посвящается 85-ию д.ф-м.н. П.П. Фирстова

Электрическая активность вулканических облаков и формирование локального электрического поля на Камчатке

Е. И. Малкин*, Н. В. Чернева

Институт космофизических исследований и распространения радиоволн ДВО РАН, 684034, с. Паратунка, Елизовский район, Камчатский край, Россия

Аннотация. В работе обобщен вклад Фирстова П. П. в экспериментальных исследованиях вертикальной компоненты E_z электрического поля атмосферы (ЭПА) в обсерватории «Паратунка» (2006–2018 гг.). На основе анализа 47 публикаций и монографии (Чернева, Фирстов, 2018) показана ключевая роль сезонного стока радона в формировании вариаций E_z. Представлены базовые модели источников поля, включая влияние пароводяных облаков, циклонов и вулканических извержений. В частности, описан проведённый лабораторный эксперимент с инжекцией пароводяной смеси из геотермальной скважины, имитирующий воздействие искусственного облака на E_z ЭПА. Приведены примеры влияния циклонической активности и эруптивных облаков от эксплозивных вулканических извержений на E_z ЭПА – интерес к этой теме Фирстова П.П. был обусловлен спецификой региона, которой является высокая интенсивность геодинамических процессов в Курило-Камчатской зоне субдукции (частые землетрясения, извержения вулканов), а также резкая изменчивость метеопараметров в связи с высокой циклонической активностью над северо-западной частью Тихого океана. Особое внимание уделено инициативе Фирстова по развёртыванию на Камчатке сети регистрации вулканических гроз. С привлечением данных сети WWLLN эмпирически подтверждён двухстадийный механизм развития вулканических гроз, а предложенная методика оценки интенсивности извержений по частоте счёта импульсного электромагнитного излучения (ИЭМИ) рекомендована как инструмент раннего предупреждения о пепловых выбросах.

Ключевые слова: регистрация атмосфериков, пеленг, электромагнитные импульсы, ОНЧ-пеленгатор молний

Получение: 23.07.2026; Исправление: 31.08.2026; Принятие: 01.09.2026; Публикация онлайн: 14.09.2026

Для цитирования. Малкин Е. И., Чернева Н. В. Электрическая активность вулканических облаков и формирование локального электрического поля на Камчатке // *Вестник КРАУНЦ. Физ.-мат. науки.* 2026. Т. 54. № 2. C. 166-200. EDN: RLPGRY. https://doi.org/10.26117/2079-6641-2026-54-2-166-200.

Финансирование. Работа выполнена в рамках государственного задания ИКИР ДВО РАН № 124012300245-2.

Конкурирующие интересы. Конфликтов интересов в отношении авторства и публикации нет.

Авторский вклад и ответственность. Авторы участвовали в написании статьи и полностью несут ответственность за предоставление окончательной версии статьи в печать.

***Корреспонденция:** E-mail: malkin@ikir.ru

Контент публикуется на условиях Creative Commons Attribution 4.0 International License

© Малкин Е. И., Чернева Н. В., 2026

© ИКИР ДВО РАН, 2026 (оригинал-макет, дизайн, составление)

Introduction

The atmospheric electric field (AEF) state is formed under the combined impact of space [1–9], meteorological [10–13] and geophysical processes [14–20], that change the conductivity of air layers at different altitudes. Multiple factors of different origin and characterized by high variability contribute to atmospheric conductivity, which causes seasonal and regional peculiarities in electric field variations [21–25]. The role of these factors in ionization phenomena, occurring in the near-ground layer, is quite complicated and ambiguous. The key factors are radon emissions from the Earth crust [26–29], galactic cosmic rays (GCR) flux [30–32], photoionization [31, 33], and electrosphere potential changes [7, 34]. Effects of each of them separately are well studied. However, the question on how they jointly influence the formation of atmospheric electric field under different conditions, taking into account seasonal and regional features, remains open. Exceptions are some separate researches where complex approach is applied [7,29]. The papers [7,22] illustrate the results of the investigations of natural process impact on the formation of atmospheric electric field vertical component E_z based on Paratunka observatory (Kamchatka) data. Factors, determining its time changes, were detected; field behavior features were studied during GCR Forbush decreases and during the changes of potential differences between the Earth surface and the ionospheric lower boundary; cyclonic activity impact was assessed. Moreover, the relation of E_z with powerful geodynamic processes, such as strong earthquakes and volcano eruptions, was considered. Based on the analysis of all the data, taking into account the contributions of the factors under consideration, one of the variants of phenomenological model for atmospheric electric field was proposed.

Features of atmospheric electric field formation based on Paratunka observatory data

Brief representation of GEC

The basis of current conceptions on the global atmospheric-electric circuit (GEC) is the quasi-stationary model of atmospheric electric field developed at the end of 1970-s and known as the model (Roble and Tzur, 1986) [1, 6]. Within the framework of this model, it was assumed that atmospheric electric conductivity decreases with altitude according to the exponential law. Taking into account the surface relief and the geomagnetic field effect on the current circuit in the upper layers of the atmosphere, theoretical distributions of atmospheric electric field (AEF) in the lower layers were obtained. In this scheme (Fig. 1a) each thunderstorm cell acts as a generator with current intensity average value. The major part of this current ($\sim 80\%$) is directed almost vertically into the ionosphere, and the minor part ($\sim 20\%$) is spread in the vicinity of a cloud in the direction of the negative pole. For the alternating current, the ionosphere and the ground surface act as quasi-potential layers, thus, the current completes through the regions with fair weather, flowing downward to the Earth. The contour is closed by inverse currents from the Earth to a cloud during lightning discharges. As long as

about ~ 90% of GEC total resistance is concentrated in the ten-kilometer near-ground layer, the potential difference reaches 0.9 from its maximum value at the altitude of 10 km. As a result, the vertical electric field of a thunderstorm attenuates exponentially with altitude, making the formation of a significant potential difference in the middle atmosphere extremely difficult.

Thus, a significant part of GEC is in the lower atmosphere. This system is determined by meteorological phenomena, it is nonstationary, complicated and undergoes anthropogenic impact. An example of its description by a phenomenological model is presented on the scheme (Fig. 1b) [7, 22].

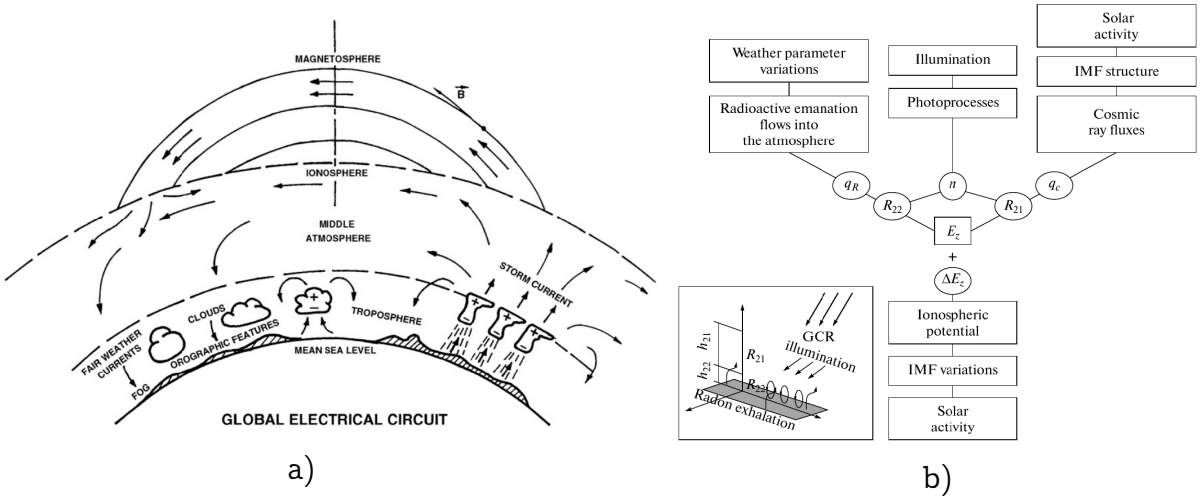

Fig. 1. Schematic diagram of various electrical processes in the global electric circuit [1]. Vector **B** shows the direction of the Earth geomagnetic field, and arrows show the directions of the current flow in the regions of the tropospheric, ionospheric and magnetospheric generators – (a). Scheme of atmospheric electric field formation processes in the presence of factors influencing its value in the surface airlayer [7, 22]. The regions of radon and cosmic ray ionization of the atmosphere are marked by R_{22} and R_{21}, respectively – (b).

Generators supporting the atmospheric electric field

Thunder clouds are not the only generators supporting atmospheric electric field, and further development of this area of research of atmospheric electricity should, first of all, include development of nonstationary models of atmospheric electric field in the near-ground layer taking into account the nature of the Earth surface (forests, deserts, glaciers, evaporation) for one-, two-, three- and multi-dimensional cases. Snowstorms, volcano eruptions, seismic activity, sunrise effect and other factors should be considered as the processes, generating uncompensated charges by the ground surface. To assess the impact of these tropospheric phenomena on GEC, their large-scale (global) representations are required. One of the ways to obtain such global data is the application of the results of atmospheric general circulation models. The estimated wind velocity, temperature, humidity, cloudiness, turbulence and other meteorological phenomena can be applied for electric parameterization in global models of atmospheric electricity.

An example of solution of a mathematical modeling problem for the atmospheric-electric circuit, taking into account different generators in the atmosphere, was illustrated in the paper [35] where stationary and nonstationary GEC models were analyzed, including thunder clouds as electric field generators and a convective current generator in the boundary layer, which modulates this field.

In order to reliably distinguish the impact of one or another generator , much attention is focused on the investigation of electric field variations, which are determined both by local and global factors. Based on the analysis of multiyear data, stationary obtained, it is possible to determine if the impact on GEC has local or global character, to estimate the change of electric field strength E_z under specified changes of the conductivity.

Empirical model of local AEF E_z according to Paratunka observatory data

An empirical model, reflecting the dependence of local atmospheric electric field on a number of natural factors (Fig. 1b), was built at Paratunka observatory based on multi-year monitoring data of the AEF E_z [7, 22]. The obtained regularities are explained by another model based on physical equations.

If we accept the atmosphere as a horizontally homogeneous medium with exponential decrease of neutral component density, and the ionized component as small impurity, then at some altitude z_e (the boundary of electronosphere with the potential U for the zero Earth potential) the neutral atmosphere on the scale of homogeneous atmospheric altitude becomes a highly conducting medium. Then a current is generated between the electronosphere and the ground. Its density j will be constant with altitude

$$j_Z = \sigma(z)E_Z(z) = -\sigma(z)\frac{dU(z)}{dz} = \sigma_0 E_{Z(0)}, E_{Z(0)} = -\frac{U}{\int \frac{\sigma_0}{\sigma} dz},$$

where $E_{Z(0)}$ is the electric field vertical component strength, $\sigma(z)$ is the air conductivity, $\sigma_0 = \sigma(0)$ is the air conductivity by the ground surface, U_Z is the electric field potential, integration is made from the ground level to the electronosphere z_e.

According to the data [36], when the total potential between the Earth and the ionosphere is 300 kV, about 270 kV falls in the lower 20-kilometer layer and only 30 kV at the altitudes from 20 to 100 km. Consequently, the near-ground layer resistance plays the critical role in the formation of the vertical current through the whole atmospheric column.

We denote the column upper part resistance, relatively constant and depending on external factors, by R_1, and the column lower part resistance by $R_2 = R_{21} + R_{22}$. R_{21} is the resistance of the layer h_{21}, the value of which is determined by cosmic rays; R_{22} is the resistance of the layer of variable thickness h_{22}, in which cosmic ray ionization is supplemented with radon ionization (inset in Fig. 1b) [7, 22]. The lower "radon" layer thickness h_{22} is determined by turbulence intensity. It is possible to estimate the voltage drop for this layer as

$$U_{22} = \frac{UR_{22}}{R_1 + R_{21} + R_{22}}.$$

On the qualitative level, we show the effect of the following most significant natural processes on AEF E_z:
– radon outflow into the atmosphere;
– cosmic ray flux variations;
– meteorological parameter variations;
– high-energy geodynamic processes;
– light and heavy ion balance change at sunset and sunrise;
– ionospheric electric current potential impact on AEF E_z potential.

Peculiarities of AEF strength regular variations at Paratunka observatory

Observations of the AEF in Kamchatka have some peculiarities:

1. Investigation of the relation of the AEF E_z with the dynamics of Rn outflow into the atmosphere under the impact of deep cyclones with sudden changes of meteorological values, having the proved impact on Rn outflow [27, 37].

2. Detailed investigation of AEF E_z diurnal variation is of high interest due to the observatory geographic location determining the difference of the local time with UT at 12 o'clock so that the time of UT-variation maximum almost coincides with the time of morning terminator during equinoxes.

Multiyear trend and factors affecting the formation of AEF E_z seasonal variation. Geophysical parameter trends over long time periods are called "secular trends". The authors of the papers [7, 22] considered comparatively short period of observations at Paratunka observatory (1998-2006), thus, it may not be entirely appropriate to refer to it as a secular trend. However, the trend in AEF E_z data obtained at Paratunka observatory turned to be close to the secular trend for Nugycenk observatory [3], which indicates presentability of the data obtained at Paratunka observatory. The trend obtained over the annual average values by the least-square method has linear dependence $E_Z = 0.021t + 888.42$ (E_Z is V/m; t is the time, days) (Fig.2a) [11].

When analyzing long AEF E_z observations, obtained at the stations of Eskadlemuir, Scotland [4], Nugycenk, Hungary and Kew, England [3], it was reliably illustrated that the secular trend has multiyear trend to AEF E_z decrease from 1920 up to the present time [11]. The possible reason affecting the trend may conventionally be the changes of heavy aerosol impurities in the air that can be associated both with anthropogenic factors and with seismic and volcanic activities in Kamchatka. However, these reasons cannot explain the regularity of the trend.

To determine the process affecting the formation of AEF E_z seasonal variation, its relation with meteorological parameters such as air pressure, temperature, snow cover level and Rn outflow into the atmosphere (Fig. 2a) was considered [11, 27, 37].

To obtain homogeneous time series with different sampling intervals, the data were averaged over half-day intervals and then by a moving average over 10 days (20 points). To decrease the contribution of noises determined by meteorological factors (rain, snow), signal limiting of +500 V/m for the upper signal limit and –200 V/m for the lower signal limit was introduced.

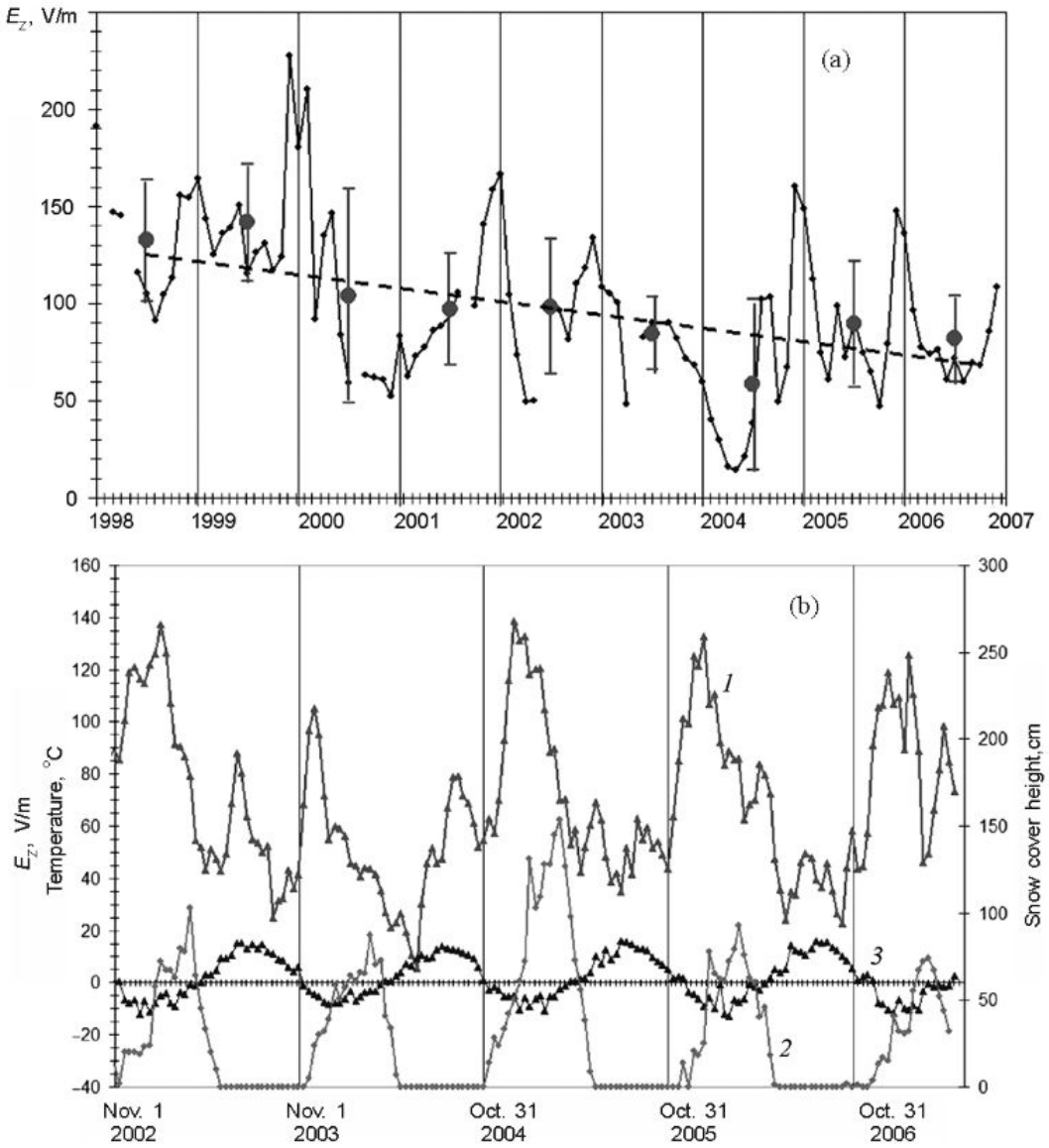

Fig. 2. Long-term linear trend (dashed line) of monthly mean (solid curve) and annual average (circles) values of AEF strength at Paratunka observatory for the sample with good weather conditions for the period 1998–2006 (a) and temporal variations of (1) AEF strength, (2) snow depth, and (3) air temperature. On panel a, vertical segments are standard deviations (b) [11, 22]

In the region of the observatory, negative average temperature remains for 5 months from November to May. During winter months, sudden changes of temperature with the range up to 15°C are observed. They are determined by the arrivals of warm cyclones which are accompanied by pressure decrease by 25 hPa. The AEF E_z seasonal variation maximum for Paratunka observatory also occurs in winter (~ 140 V/m in winter, ~ 40 V/m in summer) (Fig. 2b) [11].

The snow cover thickness maximum falls on the AEF E_z seasonal variation falling curve with the maximum correlation coefficient $r_{max} = 0.73$ with the shift of 50 days. The temperature seasonal variation minimum coincides with AEF E_z maximum for the

shift of 10 days with ($r_{max} = 0.67$), which indicates inverse relationship of these values. We can make an assumption that Rn outflow into the atmosphere increases in summer due to the increase of ground upper layer permeability that causes AEF E_z decrease. Large time shift between the snow cover thickness and the AEF E_z value indicates the fact that it has little effect on AEF E_z seasonal variation. The main role in the seasonal variation of Rn outflow into the atmosphere belongs to seasonal variations of the permeability of the ground upper layer associated with air temperature.

At the distances of less than 2.3 km from the observatory, radon volumetric activity (Rn VA) is observed in the aeration zone at the depth of one meter. The sampling rate is 2 cycles/hour [37]. Comparisong of Rn VA in the aeration zone and from the surface resulted in a qualitatively similar pattern with the correlation coefficient of 0.87, which allows us to consider the Rn VA in the aeration zone as a qualitative pattern of the dynamics of Rn exhalation into the atmosphere. Thus, it is reasonable to compare the values of the AEF E_z and Rn VA in the aeration zone over long time intervals. Due to the mass-transfer, Rn VA near the day surface decreases by more than one order relatively the depth of one meter.

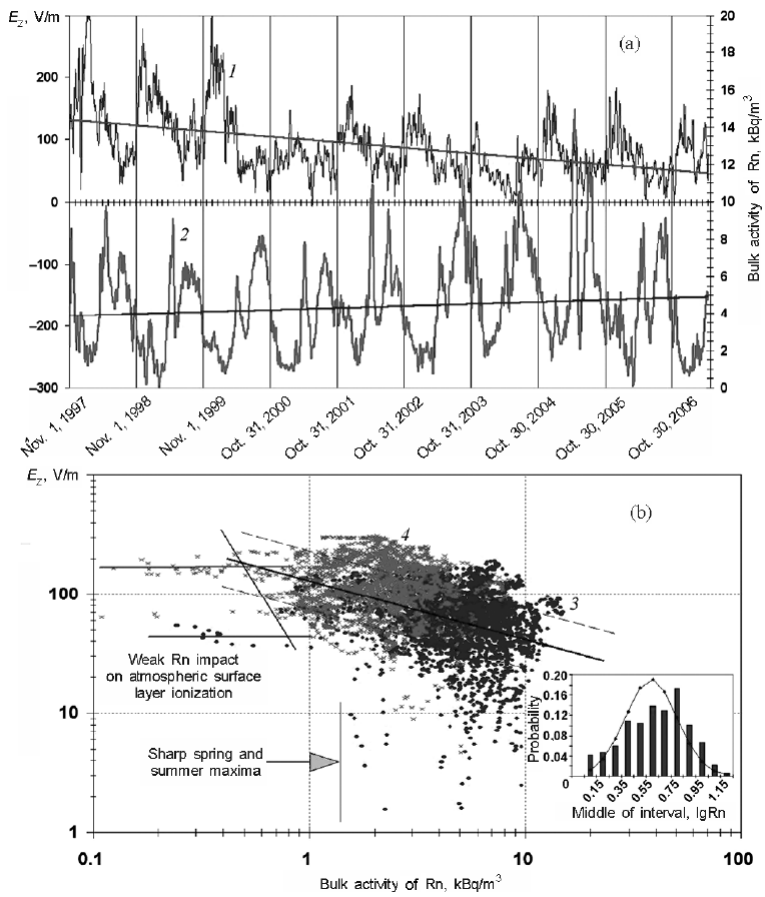

Fig. 3. (a) Seasonal variations of (1) AEF strength and (2) Rn volumetric activity in the aeration zone with the trend lines (straight lines) and (b) correlation between Rn volumetric activity of and Ez in (3) summer and (4) winter. The inset on panel b presents a histogram of the lgRn distribution according to the experimental data (bars), as well as the probability of theoretical frequencies (curve) [11, 22]

Fig. 3a [11,22] shows the curves of seasonal variations of the AEF E_z and Rn VA (for the period 1997 – 2007), which are satisfactorily approximated by the seasonal model with a trend [27].

Two maxima, spring (May) and summer (August) ones, are typical for the Rn VA seasonal variation. The sudden increase in Rn VA in May is associated with spring growth of ground water level, which causes Rn expulsion from pores and its sharp increase up to 200% and more in the aeration zone. Ground water level decrease in June causes the decrease of the level of saturation zone open surface with the shift of atmospheric column into the depth of soft sediments and, consequently, to the sudden decrease of Rn VA in the aeration zone (inflow effect). This effect manifested the most clearly after a snowy winter in 2005. Fig. 3a clearly shows that AEF E_z decreases correspond to the both curve maxima of Rn VA.

In Fig. 3b, the correlation field $\lg E_Z = f(\lg Rn)$ is presented for $E_Z > 1$ V/m of the point cloud for the whole observation period with separation of the value pairs into summertime and wintertime intervals. As a rule, the dynamic parameters of geophysical fields have logarithmically normal distribution. In the inset in Fig.3b, the probability histogram for $\lg Rn$ distribution of experimental data and that for theoretical frequencies are demonstrated.

Although the null hypothesis does not work according to the Pearson criterion, the correlation dependence $\lg E_Z = f(\lg Rn)$ was studied. A feature of the point cloud is the "jets" of small values of $E_Z < 10$ V/m. For the summer period, this is associated with the precipitation during which, as a rule, small values of Ez are observed.

Taking account of the limits demonstrated in Fig. 3b, the dependence $\lg E_Z = f(\lg Rn)$ can be described with the linear relationship estimated by the least-squares method: $\lg E_Z = -0.40 \lg Rn + 2.05(0.27)$ (E_Z, V/m; radon volumetric activity, Bq/m^3). The correlation coefficient r for this aggregate of points is –0.39 and the test of the hypothesis on the significance of sample correlation coefficient based on the Student's distribution gave the satisfactory result. As is clear from Fig. 3,b, if the Rn volumetric activity is < 1.0 Bq/m^3, the E_Z value is constant and reaches 180 V/m in winter and 40 V/m in summer. Evidently, this value of Rn volumetric activity at the depth of one meter is limiting and if it decreases, the ionizing effect of Rn outflow does not affect E_Z in the atmospheric surface layer [11].

Peculiarities of AEF E_Z diurnal variation at Paratunka observatory. The unitary variation with E_Z increase by 20% simultaneously over the whole Earth ~ at 19:00 UT is one of the most important peculiarities of AEF diurnal variation [1]. Investigations on UT variation detection at Paratunka observatory were described in the papers [22, 31, 33]. The authors of the works [22, 31] considered the behavior of the diurnal variation for the days with fair weather conditions in annual intervals for the period 1998-2003, and diurnal variation curves depending on season. On all the annual curves, the E_Z maxima fall on 19:00-20:00 UT, which may be associated with UT variations. However, we should note that Paratunka observatory zone time leads UT by 12 hours, thus, E_Z maxim during the greater period of a year falls within morning hours coinciding with sunrise. E_Z increase during the morning terminator is explained in

different ways, which are described in the classical work (Chalmers, [10]). In the paper (Kasemir, 1956 [38]), an assumption was made that exchange layer generator may exist in the near-ground atmosphere. Its activity is associated with solar radiation, increasing the contribution of the charge convective transfer and "cleaning"the atmosphere.

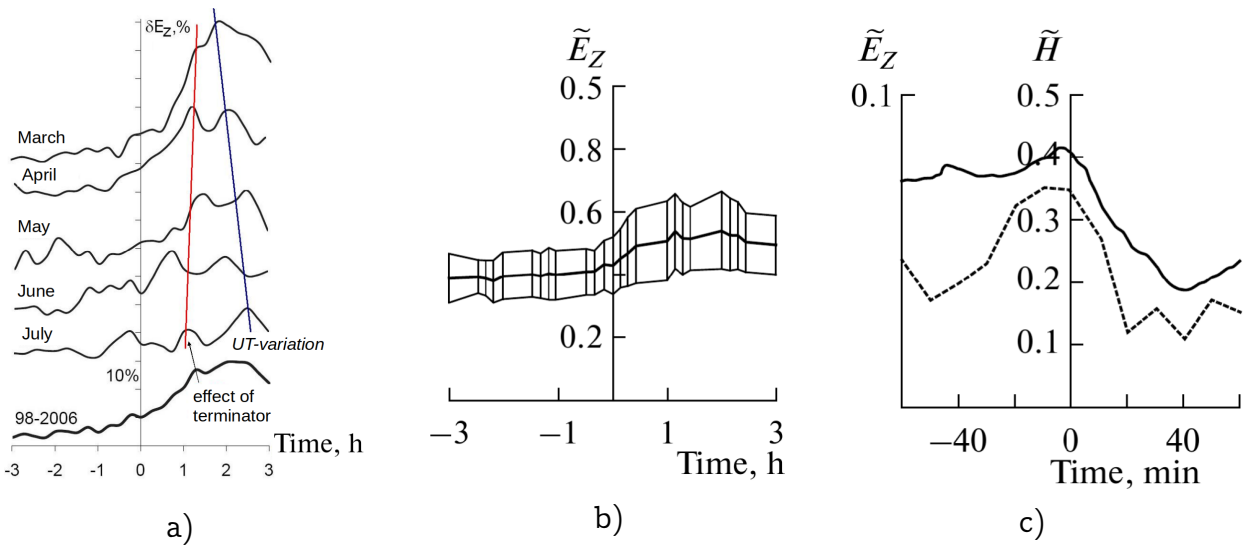

Fig. 4. Separation of the morning terminator effect and UT variations in the AEF E_Z at Paratunka observatory. Sunrise time is taken as zero (a). Separation of the sunrise effect on the AEF by the method of epoch superposition with rms errors (thin curves). In the calculations, 203 events during the days with fair weather were used; the large errors are connected to the use of data for different seasons (b). Separation of AEF variations (c) associated with geomagnetic disturbances (solid curve corresponds to H component of the Earth magnetic field and the dashed one is E_Z), the beginning of the bay in geomagnetic variations in the time range near midnight is accepted as the epoch start; the values are normalized in respect of the maximum [7, 22]

In order to detail the E_Z diurnal variation at Paratunka observatory, the maximum in diurnal variations during fair weather conditions was investigated for 2005. Depending on season, it changed from 18:00 to 21:00 UT. This apparently indicates the fact that the diurnal variation at Paratunka observatory is formed under the impact of the planetary UT variation and the local peculiarities at the recording site, such as the morning terminator (Fig.4 [7, 22]).

To separate the impacts from the UT variation and morning terminator on E_Z diurnal variation, calm days with fair weather conditions were selected from March to July within the period of 1998 – 2006 when the terminator effect should manifest the most clearly. The total number was 203 days: March - 48, April - 46, May - 35, June - 42, July - 32. The intervals of 6 hours, including 3 hours before and 3 hours after sunrise, were considered. As it is clear from Fig.4a, two maxima are distinguished within the time interval of 3 hours after the sunrise. In March they almost merge into one with the relative amplitude up to 40%. In June-July they form two maxima spaced by one hour and a half with the amplitude of 20%, which confirms the influence of the two factors on the formation of AEF E_Z diurnal variation. Curves normalized to the maximum value

were plotted by the epoch superposition method. The root-mean-square deviation of the average values did not exceed 14% (Fig.4b) .

The ionospheric potential difference effect on atmospheric electric field. In the papers [7, 22], based on the interpretation of Paratunka observatory experimental data, it was illustrated that ionospheric nonequipotentiality (which suffers the impact of the magnetospheric potential occurring during solar wind kinetic energy transformation) is reflected in AEF E_Z variations. It was shown theoretically in the paper (Park, 1976 [39]) that ionospheric potential may contribute up to 10 V/m into the AEF E_Z near the auroral zone. Later it was confirmed at Vostok station in Antarctica [32, 34]. The epoch superposition method with zero point at the beginning of midnight geomagnetic bays (normalization to the maximum) made it possible to determine the AEF E_Z responses on solar flares with 1-2 day delays based on the measurements at Zugspitze observatory (Reiter, 1969 [40]). Ionospheric potential gradients generate intensive currents in the dynamo-layer, the highly conducting region at the altitudes of 100-120 km (maximum at 107 km). Processing of 37 geomagnetic bays at Paratunka observatory (Fig.4b) [7,22] allowed us to distinguish the "ionospheric"variation composing about 5% from the background level of 120-140 V/m that is out of the framework of statistical errors and is quite a detectable effect.

Effect of Forbush decrease of GCR intensity in E_Z. As the analysis of Magadan (IKIR FEB RAS) monitor data processing showed, Forbush decreases of galactic cosmic ray intensity on the stable background of particle counting are from 3 to 10% and are quite reliably detected. We should note that the GCR are characterized by isotopic distribution in space and high time stability (diurnal changes do not exceed $\pm 2\%$), thus the relation with geophysical parameters becomes evident during flux sudden decreases caused by solar and geomagnetic disturbances, so called Forbush decreases. In the paper (Märcz, 1997, [30]), based on the data from the Nagycenk observatory (Hungary, 1962–1994) positive correlation between these decreases and the AEF E_Z variations was determined. In the review (Tinsley, 2004, [41]), the paper (Märcz, 1997) was accurately analyzed and it was concluded that the performed researches were reliable. During strong Forbush events, the AEF E_Z decreases by 5-10% within two days after the decrease beginning (though GCR flux decrease occurs faster), and then recovers within 5-10 days. The AEF E_Z recovery phase lasts for 4-5 days, that almost coincides with the recovery time for the GCR intensity.

It is not easy to detect the Forbush effect in the AEF E_Z variations. The reason is the prominent influence of the processes in the atmospheric exchange layer on the electric field during clear cloudless weather, which increases data scattering. Moreover, long periods of fair weather required for observing the AEF E_Z recovery phase (about 5 days), occur rarely. Nevertheless, in some cases synchronous decrease of the AEF E_Z with GCR Forbush decrease manifests quite clearly. Days with Forbush decreases were selected for the analysis at Paratunka observatory based on the data of Magadan neutron monitor for the period 1998-2007. Then 21 episodes with fair weather conditions (FWC) were selected from them. Almost in all these cases, the FWC in Kamchatka lasted less

than the 5-day recovery time for the AEF E_Z known on the basis of the Nagycenk observatory measurements.

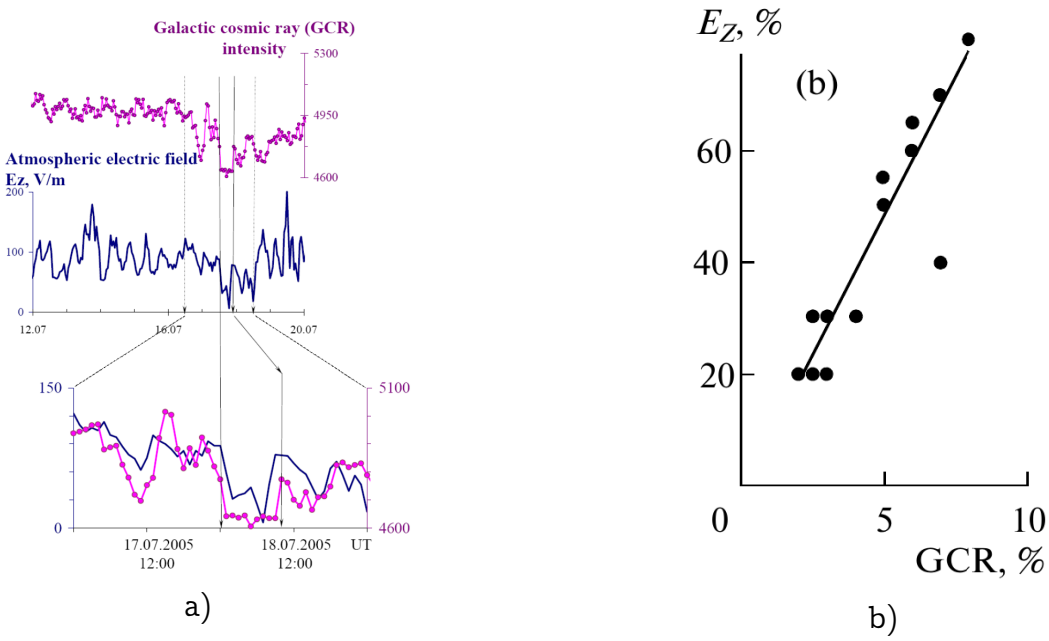

Fig. 5. GCR Forbush decreases (Magadan) and E_Z variations recorded at Paratunka observatory in July 2005 – (a). Dependence of E_Z decrease on Z(0) decrease in cosmic ray intensity during Forbush decreases – (b).

Fig. 5a shows two the most bright examples where GCR Forbush decrease and the AEF E_Z decrease were recoded simultaneously.

For 18 cases, when the decreases in the GCR and E_Z were recorded quite clearly, the dependence $E_Z(\%)$=9.64 GCR(%) – 0.72 was obtained by the least square method. As can be seen in Fig.5b, GCR decrease by 3-10% causes significant decrease of E_Z by 20-80 %.

Thus, it is possible to detect Forbush effects (GCR intensity fall) and solar terminator in atmospheric electric field variations at the background of universal (UT) variations only during complex analysis of geophysical data. Regional differences in field variations are associated not only with weather factors but with the intensity of radon inflow into the atmosphere as well, which in its turn depend on a number of atmospheric and geophysical processes.

Short-term disturbances in the AEF E_Z under the impact of separate high-energy natural phenomena

AEF E_Z changes under the influence of cyclonic activity

At Paratunka observatory, the cyclonic activity is monitored by recording atmospherics (thunderstorm electromagnetic radiation) with a VLF direction finder [11, 42]. According to the observations, powerful tropical cyclones, moving from the south-western direction, change the parameters of the lower atmosphere significantly.

Cyclone influence on some parameters of geophysical fields during the two cyclones, generated in the area of the Pacific ocean on January 8, 2002 and arrived to Kamchatka peninsula, are described in the papers [11, 22]. This cyclonic activity is of great interest due to its unusualness and to the fact that an effect was discovered in the AEF E_Z data. This effect is caused by different simple configurations of volumetric charges in the atmosphere taking into account the reflection of the initial charge in the ground, which was described in the paper [22, 44]. It is clear from Fig.6-I, where the cyclone motion trajectory is illustrated according to Kamchatka UGMS data, the both cyclones approached the Kamchatka coast two days later [43].

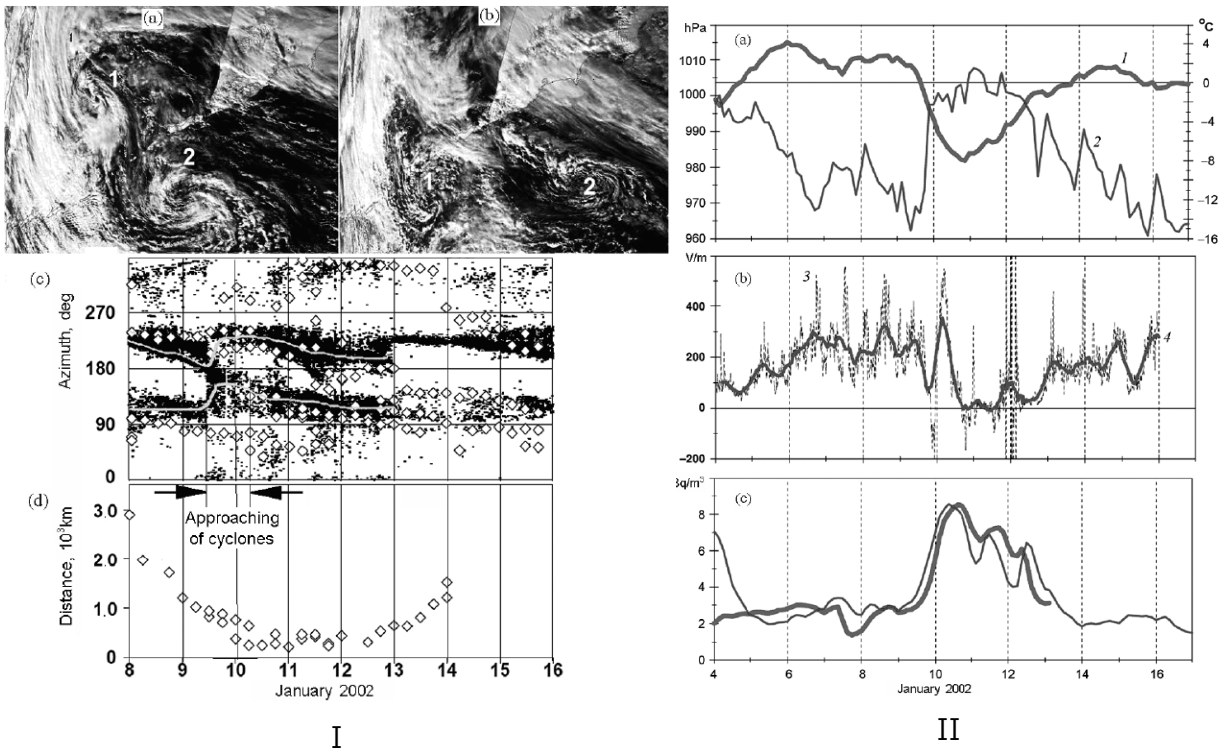

Fig. 6. I – Satellite images of the cyclones in the Pacific Ocean area on (a) January 12 and (b) January 13, 2002, (c) the azimuthal distribution of lightning discharges and cyclone centers, (d) the distance from the cyclone centers to Paratunka observatory. The numerals in Figs. I-a and I-b are the centers of cyclones. Other explanations are given in the text; II – (a) Temporal variations of (1) surface pressure, (2) air temperature, (b) AEF strength (3, instantaneous values with the sampling rate of six cycles per hour; 4, values averaged for 10-hour intervals), and (c) Rn volumetric activity from the data of two observational points

Fig.6-Ia,b shows the images from NOAA satellite at the beginning of the day on January 11-12, 2002. Two cyclonic vertexes are distinguished at the distance of ± 400 km from Paratunka observatory. They moved from the south-west to the north-east under the influence of an anticyclone front.

The cyclones motion on January 8-16, 2002 is well traced by atmospherics azimuthal distribution based on the direction finder data. In Fig.6-Ic, the light lines show the atmospherics density centers that trace the changes of cyclone central part azimuths. It is clear that on January 9, in the middle of the day, the cyclones approached each

other and collided. The distance from Paratunka observatory to their centers on January 10-12 was estimated as about 100 km (Fig.6-Id).

The meteorological parameter dynamics (air pressure, temperature and precipitation) at Paratunka observatory on January 4-17, 2002 is shown in Fig.6-IIa. From 14:00 on January 9, sudden decrease of pressure and simultaneous increase of temperature were recorded. By the end of the day on January 10, air pressure fell by 30 hPa, and air temperature increased from -15°C to 0°C. At the end of the day on January 12, the snow fall (powder snow) caused strong disturbances of the AEF E_Z illustrated in Fig.6-IIb.

Based on the data of Fig.6-IIc, the bay-like decrease of the AEF E_Z on January 10-13 is explained by the increase of radon outflow into the atmosphere. At two sites near the Paratunka observatory the volumetric activity of the underground radon synchronously increased by 4 times (from 2 to 8 kBq/m^3). Such a significant increase of radon outflow (Rn VA) is caused by the "suction"effect due to atmospheric pressure drop and increase of rock permeability during temperature growth. The increased radon flux intensified the near-ground layer ionization and its conductivity, which caused AEF E_Z decrease by almost 200 V/m. The correlation coefficient between the Rn VA and the AEF E_Z is equal to –0,43 (0.3 for the significance level of 95%).

Within the time interval from 12:00 on January 9 to the end of the day on January 10, when the cyclone front passed over the observation region, interesting dynamics in the AEF E_Z was observed. It is clear from Fig.6-IIb, convergence of the cyclone fronts first caused sudden decrease of the AEF E_Z up to –200 V/m, and then, on January 10, its decrease up to 500 V/m. After that, at the end of the day on January 10, the AEF E_Z decreased again sharply and remained at the low level almost until the middle of the day on January 12.

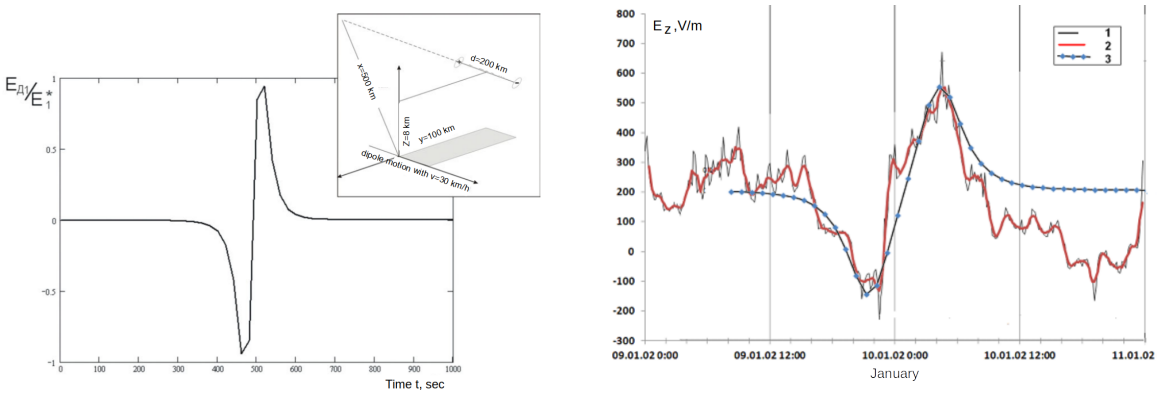

a) b)

Fig. 7. The geometry diagram of the supposed dipole formed during the interaction of two cyclones and its movement relative to the recording points (a), dynamics of the AEF E_Z on February 9-11, 2002 (b). 1 - original data, 2 - averaged by a moving average over three points, 3 - calculated curve

The AEF E_Z behavior turned to be similar in form to the basic model of the field from horizontal dipole moving along its axis (Fig.7a). This gave grounds to suggest that

when cyclones approach each other, friction between large snow-air masses generated electric dipole, which motion was recorded at Paratunka observatory.

The parameters of the dipole structure were determined using satellite images and data on the location of lightning. The height is about 8 km, the axis is oriented along the direction of movement, the distance between the charges is 200 km, and the movement speed is ~30 km/h. The initial distance to the dipole axis from the recording point was 100 km (Fig. 7a). Based on the observed scales, the volumetric structure of the electrical charges in the thunderstorm cells can be neglected, and they can be considered as point charges. Taking into account the adopted parameters, the calculation results presented in Fig. 7b showed that the curve constructed using the model agrees satisfactorily with the experimental curve, which is presented in dimensionless units according to the formula $E_Z = \frac{2qz}{4\pi\varepsilon_0[z^2+y^2]^{3/2}}$ [22, 44]. Based on the accepted parameters, it can be concluded that the charge of this aeroelectric structure, formed by two adjacent cyclones, is, to a first approximation, q ~1200 C. According to the VLF direction finder data, lightning discharges were recorded throughout the entire dipole registration period, which indicates the action of a thunderstorm generator that maintains the calculated charge value.

Investigation of electric parameters of artificial steam-water clouds

To investigate the aeroelectric structures, arising in steam-water clouds (SWC), ground observations of atmospheric-electric parameters were carried out at the times of ejections of steam-water mixture (SWM) formed during well startup of Mutnovskoe field [22,43,45]. It was expected that after the well opening, a SWC with local volumetric charge is formed at low altitude and its signal in the vertical component of the AEF E_z will be recorded by the ground. The experiment was aimed at two tasks:

1) verification of the hypothesis by Sorokin et. al. (2001) [46] that decrease and even sign change occurs in the AEF E_z before earthquakes, which is determined by the transportation of charged aerosols along tectonic faults;

2) approximated modeling of aeroelectric structures which are formed during volcanic eruptions.

First observation cycle in October 2004 and September 2006. During this period, five startups of wells were performed. The experiments are mainly described in the papers [43, 45]. AEF E_z strength was measured in the close proximity from deep wells (h>1000 м) opened for the observation time. Steam-water mixture (SWM) with different steam content was released into the atmosphere from the wells. In 2004, the experiment was realized on three wells (42, 17, 53), and in 2006, the experiment was repeated on the well 42 and made on the well 016 with very high steam content ~ 97%.

Fig.8-I shows some fragments of SWM injection into the atmosphere. The experiment was made as follows. When the well 42 was opened, a steam column of 15–20 m high arose. It was blown by wind into a cloud with the volume of ~ $10^3 m^3$.

A fluxmeter was installed at the distance of 10-60 m from the well, both on the leeward and windward sides. Each cycle included 10-minute record of the background, then 10-minute record of the parameters of the SWC formed after opening the well

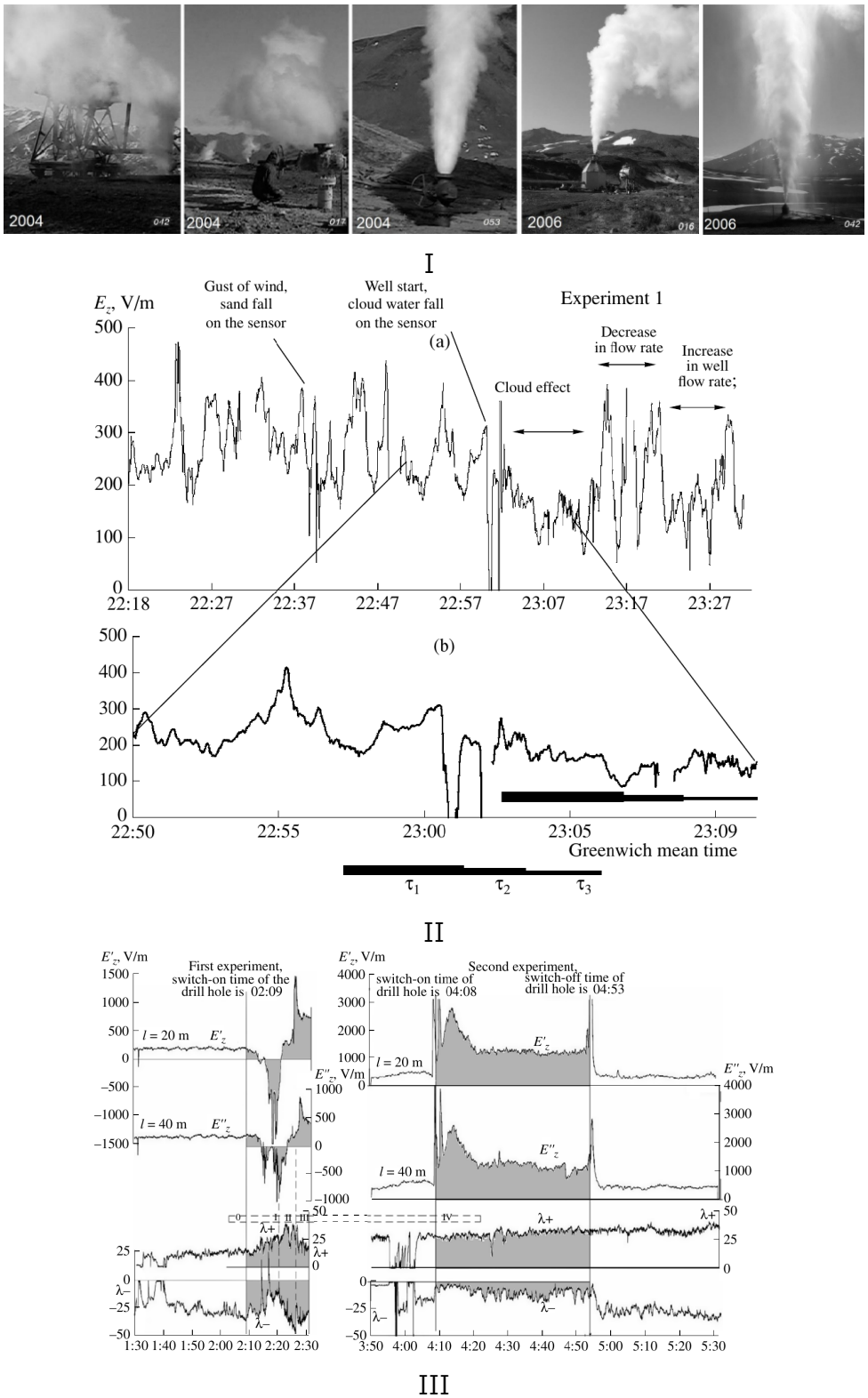

Fig. 8. I – General view of experiments on forming a steam–water cloud (SWC) at wells in 2004 and 2006. 1 – (a), 2 – (b), and 3 – (c); II – Temporal behavior of E_Z (V/m) at well 1 – (a). The moments of SWC formation, beginning of E_Z decrease, termination of rapid field relaxation, and period of slow relaxation are recorded — (b); III – Results of E_Z, λ_+, and λ_- measurements at two thermal wells [43, 45]

valve. Then the instrument was moved to another position and the cycle was repeated. The measurements lasted for about one hour for one well.

In 2006 the experiment was extended. The AEF E_z parameter was recorded by a complex consisting of three Gradient MZ fluxmeters and Electroprovodnost-2 sensor for air electric conductivity allowing us to record air positive and negative electrical conductivity. One fluxmeter was installed in close proximity from the well at the upper platform of the protecting casing. Other two fluxmeters were placed at the distance of 20 and 40 meters from the well. Electroprovodnost-2 recording system was located 20 meters from the well. Measurement results are shown in Fig.8-II,III.

When the valve of the well 042 was opened (steam-water mixture flow rate $Q \approx 93$ kg/s, humidity $\chi = 19\%$), the background value of the AEF E_z vertical component, which had been 200–400 V/m, decreased by about two times after τ_1=250 seconds. After that, slow recovery was observed for about τ_2=100 (Fig.8-IIa). At the less productive well 017 ($Q \approx 19$ kg/s, $\chi = 32\%$), the AEF E_z field reaction was weak. The decrease did not exceed 50 V/m, and the delay time τ_1 was less than 50 seconds (Fig.8-IIb). The cloud here was significantly less compared to the previous case (Fig.8-I(2)).

When opening the well 053 ($Q \approx 60$ kg/s, $\chi = 20\%$) a steam-water cloud with the volume of about $\sim 10^4 m^3$ (Fig.8-I(3)) was formed. The rate and the velocity of the mixture flow increased in time simultaneously with the forming cloud, however decrease of the AEF E_z by 250 V/m was observed during the time interval $\tau_1 \approx 100$ seconds. The time of field partial recovery ($\tau_2 \approx 150$ seconds) was almost the same as in the first experiment (Fig.8-IIb).

However, just like for the well 042, the initial value of the AEF E_z was not achieved, though the tendency to its slow recovery to the initial level maintained. Results of the observations in 2006 (Fig.8-III) at the well 042 ($Q \approx 93$ kg/s, $\chi = 19\%$) showed that after the opening of the valve, the AEF E_z field decreased to –1000 V/m during 4 minutes (due to condensation) and 15 minutes after the heating, it increased to +800 V/m, that synchronously reflected in the negative conductivity λ_-. At the highly productive well 016 ($Q \approx 13$ kg/s, $\chi = 97\%$), after the well opening, the AEF E_z suddenly increased to 2000 V/m then stabilized at 1500 V/m for the decreasing λ_- and almost constant λ_+. The conclusion was made that dry steam increases the AEF E_z and humid steam decreases it.

Condensation, coagulation, crystallization and droplet breakup take place in the upward flow of the steam-water mixture and during cloud formation. This causes electric charge formation. Negatively charged aerosoles condense water more effectively than positive ones, that is why negative droplets grow faster and settle more quickly. As a result, negative charge is accumulated at the bottom edge of a cloud and positive charge is accumulated at the upper edge. This is applicable to our case during charge separation at the distance of $\sim$ 10 m. Presence of the electric charge in the steam-water clouds was confirmed by the observations of both artificial and natural aerosol formations [22, 43, 45, 47].

Responses in the AEF E_z ***during the motion of eruptive clouds caused by volcanic explosive eruptions***

Separation of electric charges causing lightning takes place not only in usual rain and hail clouds but also in eruptive clouds (EC) during volcanic eruptions with high lightning activity, so called "volcanic thunderstorms" [14, 18, 19, 22, 47–55]. Remote investigation of electrostatic field in EC is a perspective way to trace their development and electrification processes.

Explosive eruptions are accompanied by complex geophysical phenomena when great masses of hot ash and volcanic gases are ejected into the atmosphere. Due to the release of geostatic pressure, the water dissolved in magma causes its fragmentation, which results in the formation of a large amount of dispersed material (pyroclastics). This material together with gases form eruptive clouds. EC electrification occurs under the influence of different physical mechanisms [16,18], and the observed lightning discharges are the evidences.

A volcanic eruption itself is a catastrophic event dangerous for people and urban territories. Monitoring of "volcanic thunderstorm"EC propagation by different methods makes it possible to warn about ash hazard in advance and to make arrangements for reducing damage. The most reliable remote means for tracing volcanic explosive activity are seismic, infrasound and lightning activity recording methods. The first one provides the data on eruption intensity and duration. The second one gives the data on the degree of the process nonstationarity. The third method races ash cloud motion based on lightning strokes. To improve the analysis accuracy, we applied satellite data, the data from the World Wide Lightning Location Network (WWLLN, http://wwlln.com). A local network for recording the lightning activity (Fig.9, [56]), arising during Kamchatka volcano eruptions, was constructed. It is similar to the network installed around the Redoubt volcano [48–50].

The reasonability of location of such a network in the region of the Kluchevskaya volcano group (Kluchevskaya Sopka, Shiveluch, Tolbachik) was shown in the paper [56]. VLF direction finders, electrostatic field sensors, synchronization systems and some additional equipment were included into the observation site instrumentation. The important task is the fundamental basis for understanding the electric nature of volcanic plumes, from the mechanism of lightning initiation near a vent to the evolution of charge structure at a distance. All together they allowed us not only to make the detailed picture of the electrification process but to suggest a practical method for monitoring eruptions based on lightning activity.

Since 2016 till 2023, Shiveluch (56°47´ N, 157°56´ E, extrusive dome height of 2500 m above the sea level) and Bezymyanniy (55.98° N, 160.59° E, height 2869 m above the sea level) volcanoes from the Kluchevskaya vocano group (Fig. 9) were the most active ones in Kamchatka.

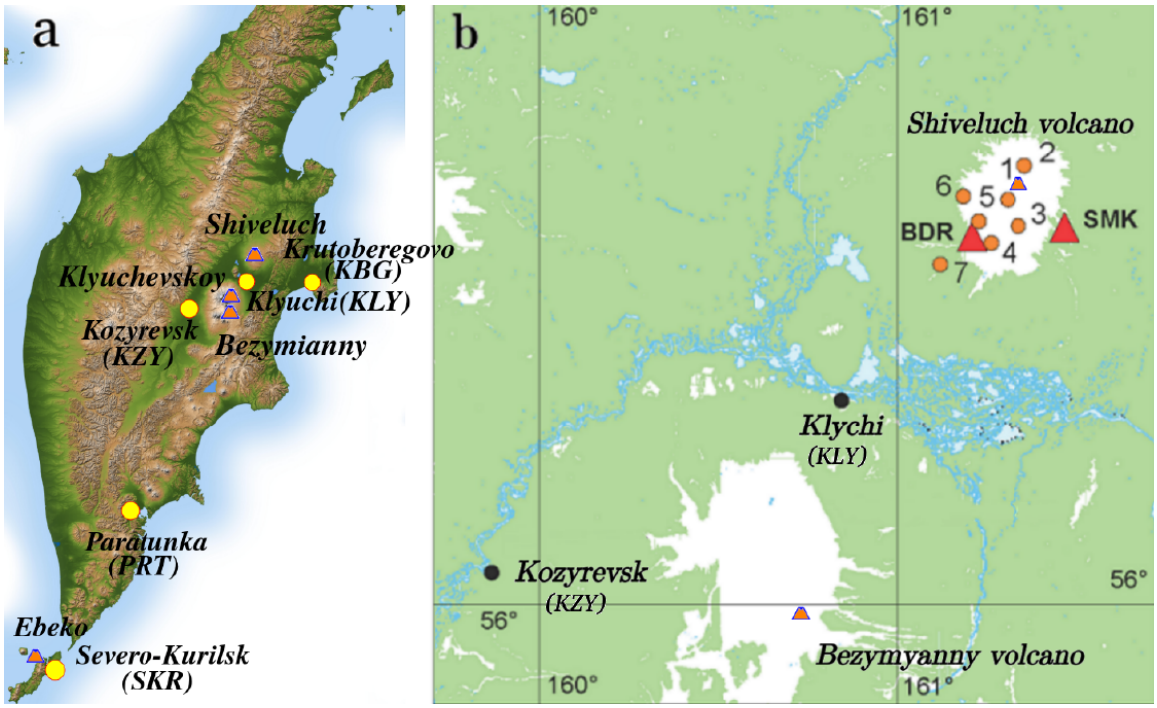

Fig. 9. Location of VLF direction finder (IKIR FEB RAS) and Shiveluch volcano in Kamchatka (a), observation points for volcanoes (CF FITS EGS RAS) in the region of the Northern group of volcanoes and discharge centers recorded by WWLLN network during Shiveluch volcano eruption on 16 November 2014 (b) [51]

Eruptions of the Northern group volcanoes

Electric processes in the volcanic clouds are an integral component of volcanic activity. Plume clouds contain a significant electric charge, which can be detected by ground instrumentation. Aerosol eruptive clouds, saturated with fine ash particles, can be detected by measuring the potential gradient vertical component of atmospheric electric field near the ground (James et al., 1998 [14]). Magma fragmentation and cloud generation process significantly contribute into the eruptive cloud electrification. In this case, charges of different sign are generated and volcanic lightning of different intensity occur. Spacial distribution of charges is provided both by gravitational sorting of particles of different sizes inside an eruptive column and plume and by triboelectric phenomena [16].

The complex approach, uniting geophysical measurements and satellite observations, gave the possibility to identify those disturbances in the AEF E_z records that are determined by volcanic (gas-ash) cloud passage during eruptive eruptions of Shiveluch and Bezymyanniy volcanoes.

Eruption of Shiveluch volcano at 10:17 on November 16, 2014 [18,19]. Before and after the eruption, the AEF E_z background value was relatively calm and equal to 60 V/m at KZy site for about 15 hours (1:25 - 16:25, November 16, 2014) (Fig.10-I).

The meteorological parameters during this period did not have any significant variations (Fig.10-Ic-e), which indicated fair weather conditions. At 10:45 first weak variations in the AEF E_z were observed.

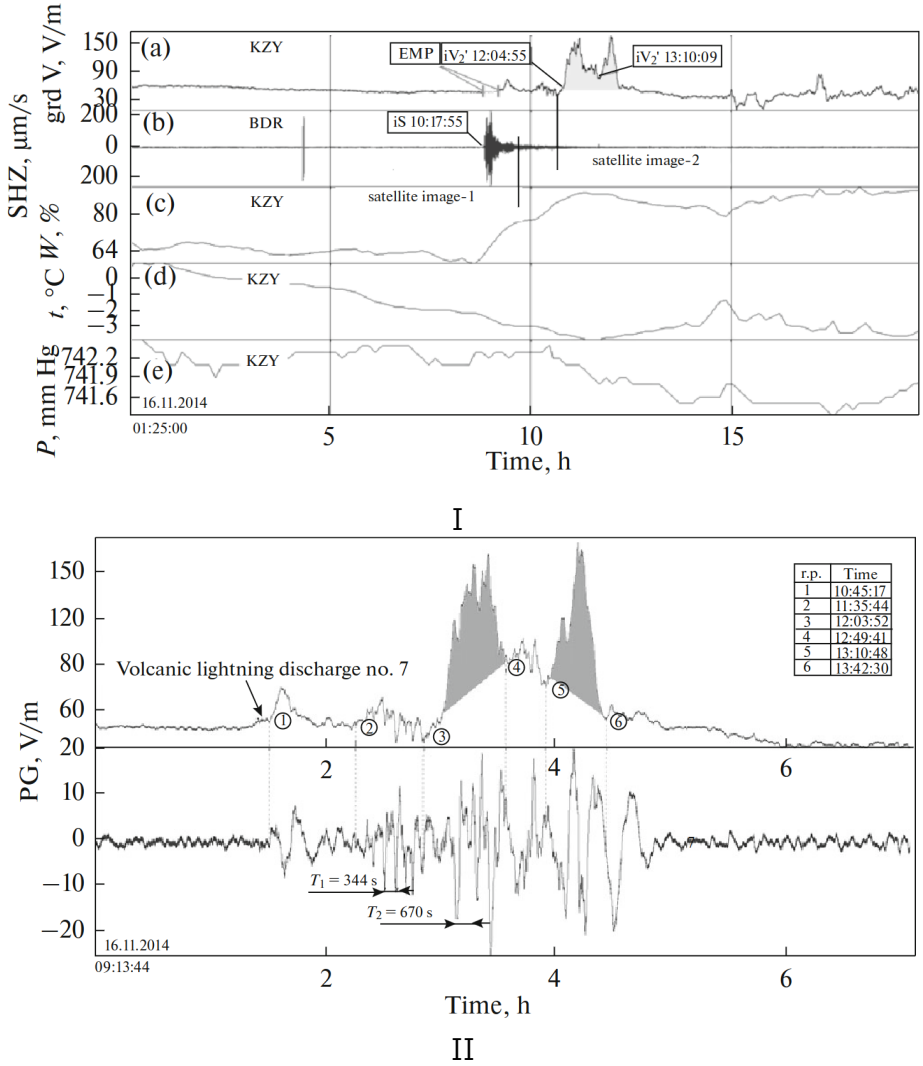

Fig. 10. I – AEF E_z at KZY (a); seismic signal which accompanied the Shiveluch volcano eruption on November 16, 2014, recorded at BDR RTSS (b); meteorological parameter at KZY (c–e) [18]; II – Fragment of AEF E_z at KZY with characteristic reference points (a); AEF E_z curve after high-frequency filtering with f_{th} = 0.0008333 Hz (20 min) (b) [19]

Almost two hours later after the eruption, clear beginnings of two anomalies (at 12:04 and 13:10) were seen with the total duration of about one hour and a half (Fig.10-Ia,b) when the AEF E_z maximum reached 170 V/m. The FWC give the basis to consider the AEF E_z variations as a sequence of electrification of the eruptive plume, the trajectory of which passed 25 km to the East from KZY site (Fig.10).

It is clear from Fig.10-IIa that higher-frequency oscillations with the amplitude ~ 10 V/m are observed for 78 minutes before the distinguished anomalies in the AEF E_z. The anomalies themselves are also complicated with high-frequency oscillations. The signal, having the duration of more than three hours, was divided into five segments and filtered by high-frequency filter with f_{th} = 0.0008333 Hz (20 min). The marked segments on the filtered signal differ quite reliably based on kinematic and dynamic parameters (Fig.10-IIb).

The signal beginning coincides with the time of the latest discharge from the volcanic lightning occurred at the distance of 90 km from KZYG and recorded by the WWLLN worldwide lightning location network. On the first segment, just like on the last one, oscillations with the period of 12-15 minutes are recorded in the records of the AEF E_z variations of high-frequency range. For the second and the third segments, oscillations with less period of 5-6 minutes are characteristic. Evidently, due to the convective instability, high-frequency oscillations of the AEF E_z are produced. They are associated with the emergence of wave motion of charged particles in the eruptive plume.

Applying the time difference between t0 and the times of arrivals of the both beginnings of the AEF E_z anomalies, the eruptive formation motion velocities were estimated as 17.7 m/s and 10.9 m/s, respectively. The coincidence of the propagation velocities of the aeroelectric structures with wind velocities at certain altitudes according to the balloon sounding data indicates the fact that the plume, propagating at two altitudes, was formed from Siveluch volcano erupion on November 16, 2014.

Shiveluch volcano eruption at 16:26 on June 14, 2017 [51,54]. It can be see in the satellite images (HIMAWARI-8, http://rammb.cira.colostate.edu/ that 34 minutes after a powerful explosion, almost round erupive cloud with the diameter of ~ 70 km was formed at the altitude of 9 km (Fig.11-Ia).

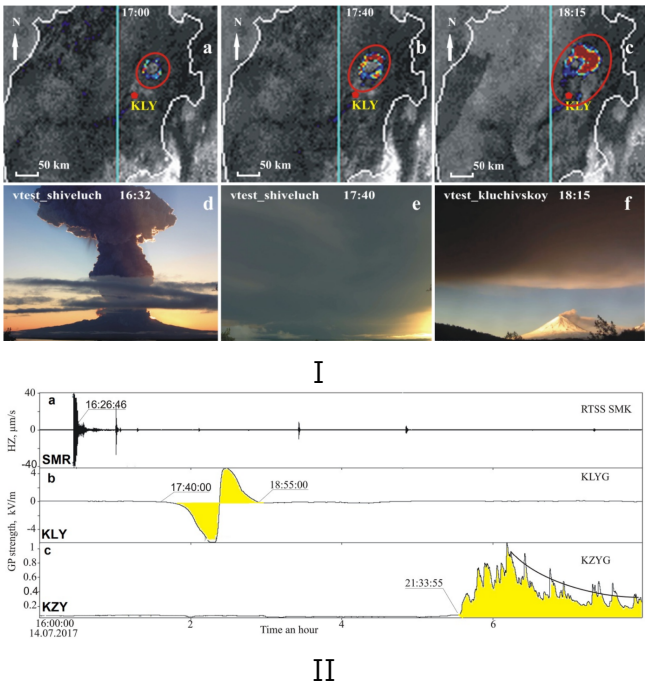

Fig. 11. I–Propagation of an eruptive cloud from Shiveluch volcano eruption on June 14, 2017 according to the data of HIMAWARI-8 satellite images (a,c) (http://rammb.cira.colostate.edu); development of an eruptive cloud recorded by a video camera at KLY (56.318439°N, 160.855891°E, the distance from the observation point to Shiveluch volcano is 45 km) (d,f) [51, 54]; II–Record fragments: ground displacement shift of the vertical component at SMK (a); AEF E_z strength at KLY (b) and KZY (c), time is indicated in the figure according to UT [51]

Then according to wind stratification, the eruptive cloud moved in the direction of Klyuchi village with the velocity of 11 m/s (Fig.11-Ia,b,c). Formation of the eruptive cloud during the first minutes of the explosive eruption beginning was recorded by a video camera at KLYG station, which monitors Shiveluch volcano activity (Fig.11-Id).

Almost an hour later, the eruptive cloud covered Klyuchi, where 100 g/m^2 of ash precipitated (Fig.11-Ie). After that, the eruptive cloud continued moving in the direction of Klyuchevskoy volcano (Fig.11-If). At 21:33 the eruptive cloud reached Kozhyrevsk village, where very finely dispersed ash weakly precipitated.

The explosive earthquake, which accompanied this eruption, lasted for about ten minutes. It was accompanied by an air shock wave that evolutionized with distance into an infrared wave and was recorded by all microbarographic channels on Kamchatka peninsula.

The favorable combination of "fair weather conditions"and wind direction during the earthquake on July 14, 2017 made it possible to record the AEF E_z response during the eruptive cloud passage over Klyuchi and Kozyrevsk villages. From the time of ash fall beginning in Klyuchi at 17:40, the AEF E_z decreased to -6 kV/m at KLY and then suddenly increased up to +5 kV/m (Fig.11-II). Significantly higher amplitude of the negative phase compared to the first case agrees with the great amount of ash of ~ 100 g/m^2 prycipitated in Klyuchi.

The form of the considered anomaly reminds the change of the AEF E_z of the horizontal dipole, the axis of which is oriented along the motion and which passes the observation site [44]. Evidently, the dipole was formed due to the eolian differentiation when large particles of ash were charged negatively in the front part of the eruptive cloud and the remaining aerosol part of the cloud was charged positively.

Dipole parameters can be estimated using atmospheric stratification and anomaly kinematic parameters. The altitude of the dipole center above the ground is $z = 9$ km with the distance between the charges of 2.5 km and the motion velocity of 36 km/hour. The dipole is formed 40 km from KLY. Based on these parameters, we estimate the dipole charge q in the first approximation by the formula $E_Z = \frac{2q}{4\pi\varepsilon_0 z^2}$, $q \approx 40$ C, where the electric constant $\varepsilon_0 = 8.85 \cdot 10^{-12}$ C/V·m.

Almost 5 hours later the eruptive cloud reached Kozyrevsk village where insignificant amount of finely dispersed ash precipitated. The fluxmeter at KZY recorded an anomaly, which form corresponded to a positively charged cloud [44]. It indicates the fact that during the eolian differentiation process, an aerosol cloud with insignificant amount of fine ash was formed.

In spite of the significant number of explosive eruptions of Shiveluch volcano, ashfalls during the eruptions at KLY were rarely observed. Thus, for accurate recording of the AEF E_z variations, observation sites should be located in the directions of the ashfall main axes formed by the wind rose.

The Shiveluch volcano weak explosion, accompanied by a slide, on December 16, 2016 at 22:31 was probably a "blowing-out"for more than 10 minutes as the result of which the eruptive cloud, formed at the height of ~ 6 km above the sea level, moved south-westward passing by the KLYG site. Whereas the ash cloud from the slide, formed

at the height of ~ 2.5 km above the sea level, passed over the Klyuchi village and caused the AEF E_z anomaly typical for cloud structures.

The powerful explosion of Shiveluch volcano on June 14, 2017 at 16:26 was a "burst"followed by a "blowing-out". The emerged eruptive cloud passed over the two sites (KLY–48 km; KZY–109 km). While in the nearest site the eruptive cloud had electric structure as a dipole, at the farthest site, the electric structure evolutionized into a negatively charged cloud due to the eolian differentiation.

Eruption of Bezymyanniy volcano at 3:39 on December 20, 2017 [57]. According to the explosive earthquake records made at the seismic stations nearest to the volcano, the eruption began at 3:39 on December 20, 2017. During the first ~ 5 minutes, seismic vibration intensity gradually increased, then suddenly arose and during the following 4 minutes the signal exceeded the dynamic range of the recording instrumentation. Then the vibration amplitude decreasded and remained unchanged for about 5 minutes and fell to the background level for about 10 minutes (Fig.12b).

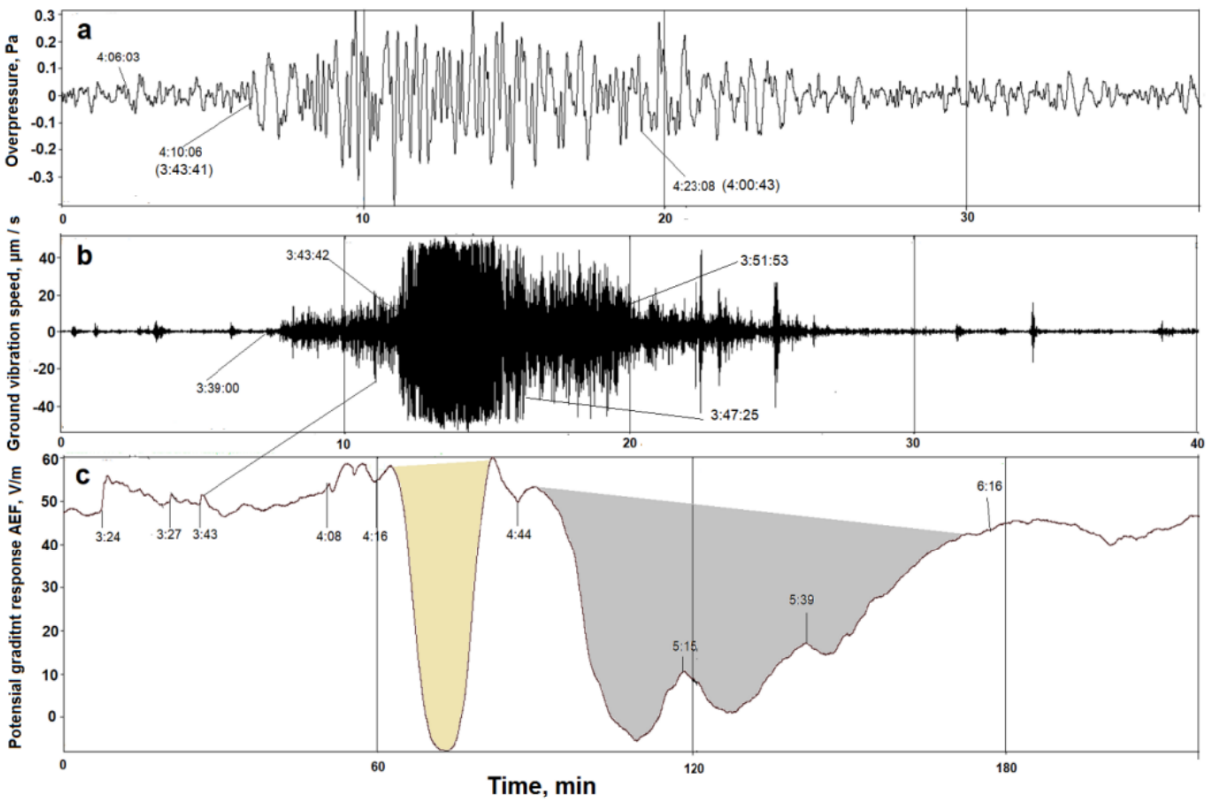

Fig. 12. Dynamics of geophysical field parameters accompanying Bezymyanniy volcano eruption on December 20, 2017: wave disturbances recorded at the infrasonic site IS44, estimated time of signal occurrence is in brackets – (a); ground vibration velocity record on the vertical component at BZW – (b) ; AEF E_z response at KLY site during EC passage – (c). The beginning of time reading corresponds to: (a) - 04:03:51, (b) - 03:31:51, (c) - 03:17:15. [57].

Turbulent column and eruptive cloud (EC) were the sources of infrasound waves in the atmosphere. These waves were recorded by the IS44 infrasound station and by KZY

observation site. Fig.12a shows the arrival times for separate wave groups recounted by the moments of their generation. The onset of the infrasound signal coincides with the beginning of the sudden increase of ground vibration velocity at BZW.

The EC ashfall axis passed ~ 20 km from KZY. Fair weather conditions made it possible to record the response from its passage with the total duration of about two hours by an electrostatic fluxmeter. The response included two bay-like signals of negative polarity with the amplitudes of 60 and 50 V/m and duration of 20 and 90 minutes (Fig.12c).

According to the VLF direction finder of IKIR FEB RAS and the WWLLN, the EC thunderstorm activity dynamics is shown in Fig.13.

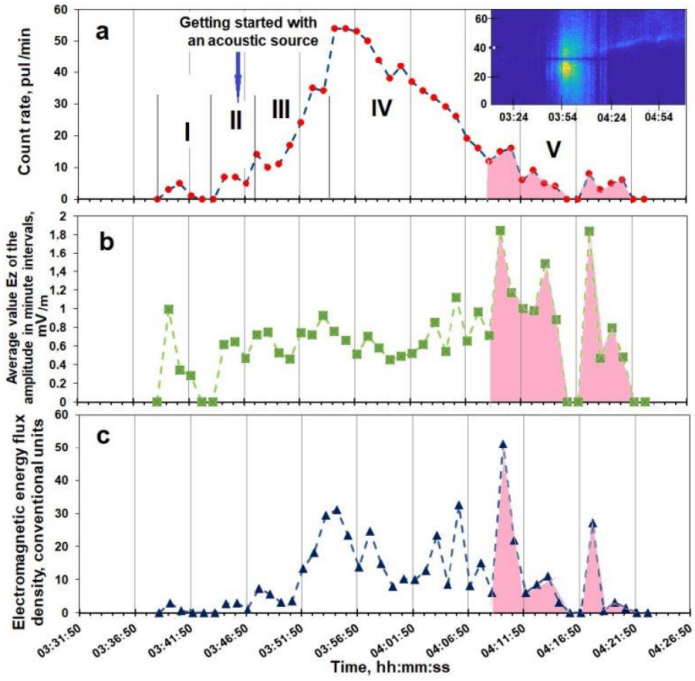

Fig. 13. Lightning activity dynamics for EC developed as the result of Bezymyanniy volcano eruption on December 20, 2017 with 1-minute sampling rate: EMP number (N) – (a); average value of EMP maximum amplitudes ($\bar{A}_{max}$) – (b); average value of EMP electromagnetic energy flow per minute ($\bar{E}$) – (c). The inset shows EMP density spectrogram from the azimuth of 0° – 60° [57]

Increased number of electromagnetic pulses (EMP) were clearly recorded for ~ 40 minutes from the direction to Bezymyanniy volcano (23.6°) (insert in Fig.13a). During the first 6 minutes (**I**), a weak increase of the EMP number was recorded in minute intervals (N) with the total number of 9 EMP.

This indicates the eruption occurrence according to the "smooth"scenario that agrees with the earthquake record (Fig.13b). All EMP had negative polarity of the first half wave (Fig.13a), that indicated vertical orientation of radiating dipole with positive pole at the bottom. The following 11 minutes (**II+III**) are characterized by N increase up to 54 pulse/min followed by a decrease during 15 minutes (**IV**) up to N =12 pulse/min. For these both time intervals, the average maximum amplitude ($\bar{A}_{max}$) was within 0.4 - 1.0 mV/m.

Some increase of N and significant increase of $\bar{A}_{max}$ and $\bar{E}$ occurred on the section V (marked by pink in Fig.13). During that period, the EC interacted with meteorological clouds spread along the Kamchatka coast [57].

Pulse electromagnetic radiation of volcanic lightning

During the observation period since 2016 up to the present time, a large volume of data has been accumulated. These data show the efficiency of remote observation methods for the eruptions of Kamchatka Northern group of volcanoes. According to the data of Kamchatka Branch of the Federal Research Center "Geophysical Survey"RAS (KB FRC GS RAS, `http://www.emsd.ru/~ssl/monitoring/main.htm`) a catalogue of the strongest events on Shiveluch and Bezymyanniy volcanoes was compiled for the period 2016–2022. About 70 eruptions of Shiveluch volcano and 13 eruptions of Bezymyanniy volcano were selected, and 75% from them caused volcanic thunderstorms radiating electromagnetic pulses recorded by the direction finder.

For the five strongest explosions of Shiveluch volcano in 2017 and two explosions of Bezymyanniy volcano in 2019 (`http://www.emsd.ru/~ssl/monitoring/main.htm`), reflected in monitoring remote methods, the parameters (Tables 1,2) characterizing the explosive eruption process were considered [51].

Table 1

Characteristics of eruptive and lightning activity during explosive eruptions on Shiveluch volcano in 2017

Date	t_0	H	A^z_{max}	Δ t	Δ t_1	C_{max}	N_1	Δ t_2	C_{max}	N_2
11.05	18:24:19	10	18.5	11.2	4	13	36	28	12	144
16.05	07:05:52	10	9.3	9.4	2	4	6	11	2	16
14.06	16:26:44	12	8.1	6.5	3	20	41	10	7	42
18.06	16:26:57	11	15.4	12.4	4	9	15	38	15	207
23.07	17:43:23	8	2.7	48.5	3	3	6	36	14	158

Table 2

Characteristics of eruptive and lightning activity during explosive eruptions of Bezymyanniy Volcano in 2019

Date	t_0	H	A^z_{max}	Δ t	Δ t_1	C_{max}	N_1	Δ t_2	C_{max}	N_2
20.01	16:05:58	15	45.4	15.2	–	–	–	19	22	206
15.03	17:12:05	16	58.5	35.4	5	32	93	51	88	1043

H – altitude of the eruptive cloud according to satellite images, km; A^z_{max} – maximum amplitude of ground displacement at KLY, $\mu m/s$; Δt – duration of a seismic record at SMK, min; Δt_1, Δt_2 – duration of the first and second phases of volcanic thunderstorms, min; C_{max} – maximum counting rate, pulse per minute; N_1, N_2 – total number of EMP recorded in the minute interval at the first and second stages of a volcanic thunderstorm.

Explosive earthquakes characterize the intensity and duration of magma fragmentation process, thus, comparison of electromagnetic and seismic radiations at

the qualitative level is the necessary requirement for understanding the development of electrostatic process in EC at the initial stage.

According to the direction finder data, the formation of eruptive clouds was accomponied by PEMR from the azimuth to Shiveluch volcano which is 25.6° ± 10° from the observation point.

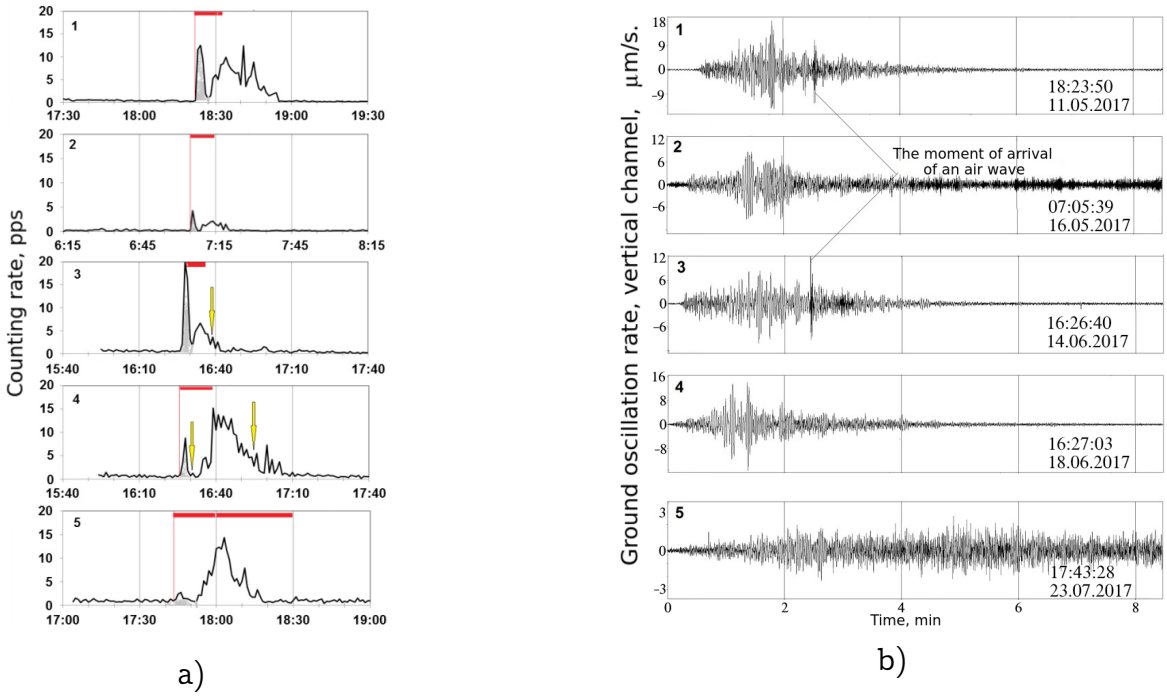

Fig. 14. EMP counting rate in minute intervals, from the azimuth of 25.6°±10° to Shiveluch volcano – (a); Records of explosive earthquakes on the vertical component at KLY seismic station – (b). Panel numbers correspond to table 1 numbers [51]

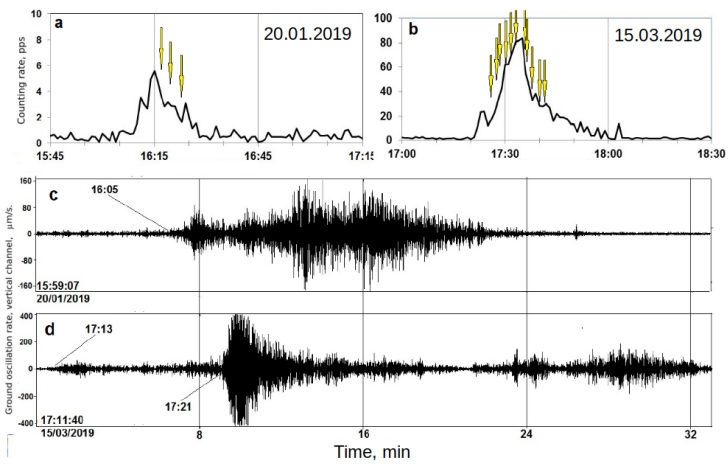

Fig. 15. EMP counting rate in minute intervals from the azimuth of 25.6°±10° to the Bezymyanniy volcano on January 20, 2019 – (a) and March 15, 2019 (table 2) – (b) record of explosive earthquakes at the seismic station, vertical component – (c, d). Arrows indicate lightning discharges recorded by the WWLLN network, red lines indicate the duration of seismic signals at SKR seismic station [51]

Fig. 14 and 15 shows the dynamics of the PEMR counting rate within a minute interval in a two-hour temporal neighborhood.

Two-stage nature of volcanic thunderstorms

For all the volcanic thunderstorms, recorded by the VLF direction finder of IKIR FEB RAS, two-stage nature of PEMR generation is typical, which was earlier detected for the eruptions of Augustine and Redoubt volcanoes in Alaska [49]. The mechanism explaining the two-stage nature on the example of Kamchatka explosive eruptions is described in the papers [51, 54, 57].

The first stage, lasting for 5-7 minutes, accompanies eruptive column formation. The second stage, lasting for 20-80 minutes, is associated with the formation and propagation of an eruptive cloud. The first stage intensity depends on explosion power and ash ejection altitude. This parameter can be associated with the following eruption scenarios:

- *«Smooth»* scenario is when an eruptive cloud is formed at the tropopause altitude and is explained by positive buoyancy of the ash-gas mixture.
- *«Rough»* scenario is explained by an explosion. In this case, the initial pulse allows the eruptive cloud to overcome the tropopause altitude.

The Fig.14,b-1 and 14,b-3 show the moments of arrival of air shock wave corresponding to the explosion, which indicates *«rough»* scenario. Just during these events, high lightning activity during the first stage of the volcanic thunderstorm was recorded.

The second stage is characterized by the number of ejected volcanic material and possible EC interaction during its passage with the clouds of meteorological origin. The second stage manifests the most brightly during Bezymyanniy volcano eruptions, the main feature of which is long duration and a large amount of erupted material (Fig 15,c,d).

To illustrate the two-stage mechanism of thunderstorm generation in eruptive clouds, we consider three events for each of Shiveluch and Bezymnyanniy volcanoes.

Table 3 shows conditional characteristics for the two stages of three the most intensive volcanic thunderstorms occurred during Shiveluch volcano eruption.

Table 3

Parameters of the three most significant events during Shiveluch volcano eruptions

Date	Time	Time 1 stage, min	Maximum counting rate, ppm	Number of pulses,	Time 2 stage, min	Maximum counting rate, ppm	Number of pulses,	WWLLN
11.05.2017	18:24	4	16	47	28	14	183	4
23.07.2017	17:43	4	3	10	26	18	205	0
21.10.2019	12:17	5	18	45	–	–	–	0

Fig. 16 illustrates the counting rage for recorded pulses of the events presented in Table 3.

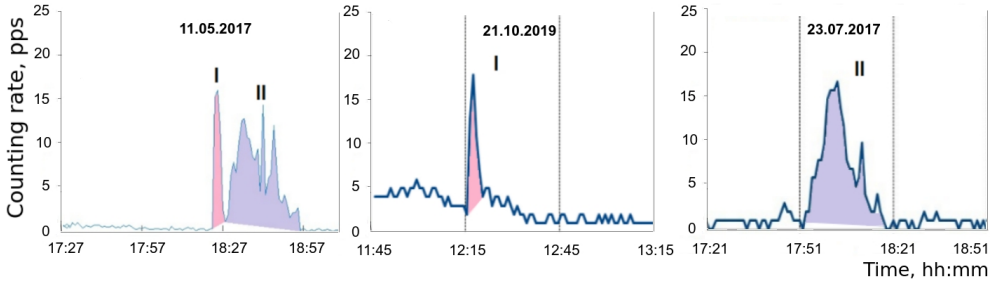

Fig. 16. Counting rate of the EMP, arriving from Shiveluch volcano, during the eruptions. UT time is shown on the abscissa, stroke count per minute is shown on the ordinate

For the Shiveluch volcano eruptions, the both scenarios of explosion development are typical, however, in most cases the *«rough»* one prevails, which is reflected in the dynamics of accompanying volcanic thunderstorms. The explosion duration on May 11, 2017 was ~ 10 min, but a shock wave was recorded after the burst, which indicates *«rough»* scenario.

According to Table 3, the total number of discharges during the first and the second stages of the volcanic thunderstorm was 28 and 183, respectively. The explosion on October 21, 2019 differed only in duration which was ~ 5 min. This indicates small volume of erupted material and, as a sequence, absence of the second phase of the volcanic thunderstorm. The eruption on July 23, 2017 occurred according to the *«smooth»* scenario. Firstly, neither infrasound waves no shock waves, accompanying the explosion process, were recorded. Secondly, the explosion duration was ~ 57 min, as the result of which there was no the first stage of the volcanic thunderstorm.

For Bezymyanniy volcano, *«smooth»* scenario is typical. This is indicated by small values of the number of the pulses recorded during the first stage of volcanic thunderstorms (Table 4), but the explosion duration results in high values of the total number of lightning occurrences recorded during the second phase.

Table 4

Parameters of the three most brightest events during the Bezymyanniy volcano eruptions

Date	Time	Time 1 stage, min	Maximum counting rate, ppm	Number of pulses,	Time 2 stage, min	Maximum counting rate, ppm	Number of pulses,	WWLLN
20.12.2017	03:39	3	5	9	54	37	781	7
15.03.2019	17:11	3	49	112	41	122	1466	11
15.03.2022	12:50	3	20	54	21	32	313	4

A peculiarity of the eruption on March 15, 2022 was a burst at 12:50, which reflected in the dynamics of the volcanic thunderstorm development in the form of the two stages with clearly defined phases one and two (Fig.17).

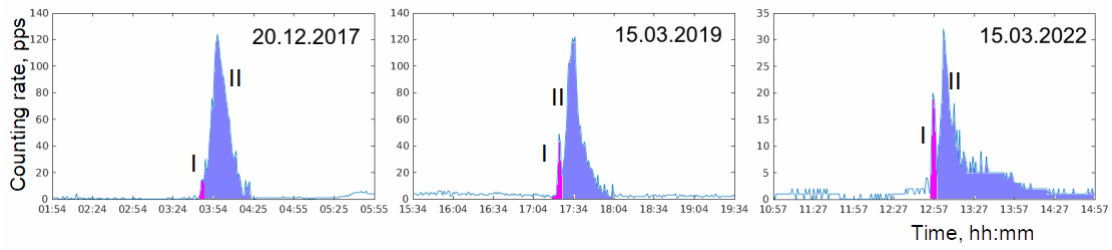

Fig. 17. Counting rate of the EMP arriving from Bezymyanniy volcano during the eruptions. UT time is shown on the abscissa, stroke count per minute is shown on the ordinate

Azimuth of the pulse radiation arrival for all the pulses of the first stage was $23.6° \pm 0.4°$, which coincided with the azimuthal direction to the volcano. The discharge maximum intensity was observed 17 minutes after the eruption beginning with the azimuth $\sim 17°$. When analyzing the initial phases of the recorded pulses it was detected that the direction of positive lightning in the dynamics of thunderstorm development shifted monotonously as azimuth decreased (the last positive pulse had the azimuth of 8.2°), whereas negative lightning occurrences were observed in all azimuthal angles corresponding to angle dimensions.

Discharge polarity in eruption dynamics and distribution of electric discharges in eruptive clouds [20, 55]. When a gas-ash stream is injected into the atmosphere due to the hydrodynamic resistance and sedimentation, fractional separation of ash particles takes place, causing accumulation of larger and, consequently, positively charged particles at the bottom of an eruptive column. This, in its turn, should initiate lightning of positive polarity. After EC development, due to a great amount of water (up to 7% of the erupted material and up to 97% of gas weight content), classic mechanisms of charge separation, characteristic to meteorological clouds, should work.

According to the data obtained during the eruptions and presented in Table 1, the majority of the charges of the first phase have positive polarity, that is the initial dipole moment of the radiating dipole is primary directed upwards (39 cases for the event on May 11, 2017, 7 cases for July 23, 2017 and 37 cases for October 21, 2019). During the second phase, the most part of the charges have negative polarity, on the average 98% from the total number of recorded discharges. This indicates opposite direction of the initial dipole moment and, as a sequence, inversions of the EC total field.

Natural observations, carried out during the Great Fissure Tolbachik eruption in Kamchatka in July-October 1975 [47], and the Sakurajima volcano (Japan) during the eruption in 1995 [52], made it possible to give qualitative description of the configuration of eruptive cloud charges (inset in Fig.18 [20]), which explains the two-stage scenario of the eruptions and shows the mechanism of impact on the whole GEC (Fig.1 and 18).

Consequently, the first phase of a volcanic thunderstorm, lasting for 5-7 minutes, accompanies eruptive column formation. The positive space charge in its lower part is generated due to fractional separation of ash particles (large fractions are charged positively, small ones are charged negatively). The pause between the phases is explained by charge separation in the upper part of an eruptive cloud.

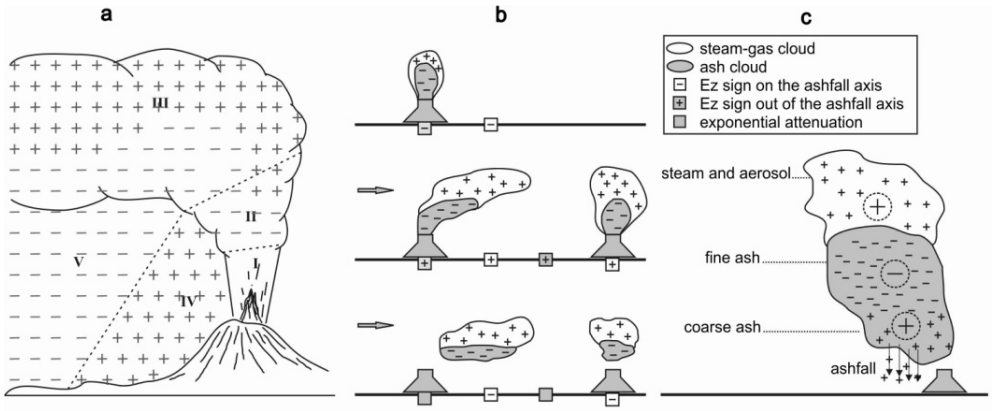

Fig. 18. Schematic models of electric structure formation in an eruptive cloud a - in the near-field zone [47]; b - schemes of charge separation during volcanic plume formation under wind effect according to [52]; c - charge separation in eruptive clouds based on natural observations on Sakurajima volcano according to [14]. I – charge separation under gravity action at the initial section during weak wind; II – cloud formation at the automodeling section under wind effect; III - plume at the floating zone; IV – coarse fraction fall area; V – tefra fall area [20, 55]

According to the paper [47], aerosols in the buoyancy zone carry positive charge generating the field opposite to that of the eruptive column. During a long eruption, aerosol number grows, space charge increases and the resulting field, generated by an eruptive column, changes its sign to the opposite.

Discussion

The obtained data significantly deepen our understanding of the physics of explosive erupions and of how electrostatic processes influence the eruptive cloud dynamics. Analysis of the measurements, taking into account the considered factor effects and the stored knowledge, makes it possible to imporve the phenomenological model of atmospheric electric field, which was earlier suggested in the paper [7].

In this context, high-altitude lightning discharges deserve our close attention. They generate atmospherics and whistling atmospherics (whistlers) in the radio range and sprites in the optical rage. Such discharges occur during intensive lightning activity of both meteorological and volcanic origin connecting electric processes in the lower and upper layers of the atmosphere and lithosphere into a single system. Height discharges play a significant role in the formation of ionospheric electric potential since they provide pulse discharge of its charge, locally releasing a part of its potential energy. This is precisely their key difference from ground lightning.

The current, generated in the high-altitude discharge, penetrates into the ionosphere and excites electromagnetic oscillations (Fig. 18) [55]. These oscillations propagate along the magnetic field lines and, as they rise higher, they undergo frequency dispersion due to the decreasing role of plasma particle collisions and are recorded at a receiving

point as whistlers. This mechanism of whistler generation was confirmed by satellite experiments with plasma jet ejection into the magnetosphere [58].

The relation between high-altitude discharges and whistlers has been investigated for a long time, however problems remain. It is difficult to distinguish high-altitude discharges themselves at the background of intensive fluxes of near-ground lightning and it is difficult to locate whistlers generated just by these discharges [59, 60].

High-altitude discharges can be single or paired with a preceding near-ground lightning. The second case simplifies the search for high-altitude discharges but at the same time, single discharges remain unnoticed.

Thus, the central scientific task, following from all the abovesaid, becomes systematic accumulation of data, detailed study and detection of the relations between high-altitude electric discharges, whistlers, ionization processes and meteorological parameters. This is the basis for constructing a new multifactor GEC model.

Conclusions

According to the data of multiyear monitoring of the AEF E_z at Paratunka observatory (Kamchatka), the effect of the following natural factors has been illustrated: radon seasonal emanation (annual variation ~100 V/m), diurnal maximum during evening hours (terminator effect) and Forbush decreases of cosmic rays (AEF E_z decrease by 20–80%). During the passages of cyclones and eruptive clouds from Shiveluch volcano, anomalies of the AEF E_z of different sign (negative nearby, positive at the distance) were recorded. Experiments with steam-water mixture ejections at Mutnovskoe field showed that humid steam decreases the AEF E_z, dry steam increases it, the response depends on sensor location.

In the gas-ash stream of an eruptive cloud, due to resistance and fall-out, large positive particles of ash are accumulated at the bottom of a column causing positive lightning. In a well-developed eruptive cloud, due to abundance of water (up to 7% of the mass, up to 97% in gases), standard meteorological mechanisms work. All the eruptions have two stages. The first stage (5–7 min) is the column formation with positive charge at the bottom (large «+», small «–»). Charge separation at the top of a cloud occurs when positive aerosols of the buoyancy zone create an opposing field. During a long eruption, the aerosole number grows, space charge increases and the column resulting field changes its sign. Qualitative models of EC charges explain the two-stage nature of eruptions.

The suggested phenomenological model of local AEF requires the correction of the scheme for the global electric circuit taking into account the obtained knowledge.

Acknowledgments. The authors pay tribute and express their gratitude to the great Russian scientist P.P. Firstov. He initiated many experiments and analysis of the continuous series of the data published in the papers [7, 11, 18, 19, 22, 27, 37, 44, 51, 56]. Under his scientific supervision, observation results were analized and modeled with high degree of reliability. The obtained knowledge has large scientific potential which is confirmed by two defended dissertation works by Akbashev R.R. (http:

//www.imgg.ru/ru/dissertations/23) and Malkin E.I. (https://disser.spbu.ru/zashchita-uchenoj-stepeni-spbgu/1447-malkin-evgenij-ilich.html) followed by the published papers [20, 55].

Abbreviations

EC	Eruptive Cloud
EMP	Electromagnetic Impulse
WWLLN	World Wide Lightning Location Network
AEF E_z	the vertical component of the Atmospheric Electric Field
PEMR	Pulsed ElectroMagnetic Radiation emissions
GCR	Galactic Cosmic Rays
GEC	Global atmospheric-Electric Circuit
Rn VA	Radon Volumetric Activity
FWC	Fair Weather Conditions
UT	Universal Time
VLF	Very Low Frequency

References

1. Roble R. G.,Tzur I. The global atmospheric-electrical circuit / *The Earth's Electrical Environment.* Washington, D.C., National Academy Press, 1986, pp. 206–231 DOI: 10.17226/898.
2. Tinsley B. A. Influence of solar wind on the global electric circuit, and inferred effects on cloud microphysics, temperature, and dynamics in the troposphere, Space Science Reviews, 2000. vol. 94, pp. 231–258 DOI: 10.1023/A:1026775408875.
3. Märcz F., Harrison R. G. Long-term changes in atmospheric electrical parameters observed at the Nagycenk (Hungary) and the UK observatories at Eskdalemuir and Kew, Ann. Geophys., 2003. vol. 21, pp. 2193–2200 DOI: 10.5194/angeo-21-2193-2003.
4. Harrison R. G. The global atmospheric electrical circuit and climate, Surveys in Geophysics, 2004. vol. 25, no. 5-6, pp. 441–484 DOI: 10.1007/s10712-004-5439-8.
5. Aplin K. L. Atmospheric Electrification in the Solar System, Surveys in Geophysics, 2006. vol. 27, no. 1, pp. 63–108 DOI: 10.1007/s10712-005-0642-9.
6. Singh D., Gopalakrishnan V., Singh R. P., Kamra A. K., Singh S., Pant V. The atmospheric global electric circuit: An overview, Atmospheric Research, 2007. vol. 84, no. 2, pp. 91–110 DOI: 10.1016/j.atmosres.2006.05.005.
7. Ponomarev E. A., Cherneva N. V., Firstov P. P. Formation of a local atmospheric electric field, Geomagnetism and Aeronomy, 2011. vol. 51, no. 3, pp. 402-408 DOI: 10.1134/S0016793211030145.
8. Rycroft M. J., Nicoll K. A., Aplin K. L., Harrison R. G. Recent advances in global electric circuit coupling between the space environment and the troposphere, Journal of Atmospheric and Solar-Terrestrial Physics, 2012. vol. 90-91, pp. 198–211 DOI: 10.1016/j.jastp.2012.03.015.
9. Williams E., Mareev E. Recent progress on the global electrical circuit, Atmospheric Research, 2014. vol. 135-136, pp. 208–227 DOI: 10.1016/j.atmosres.2013.05.015.
10. Chalmers J. A. *Atmospheric Electricity. – 2nd ed.*. Oxford – New York: Pergamon Press, 1967. 515 pp.
11. Cherneva N. V., Firstov P. P. Weather factor effects on electric parameters in the lower atmosphere, Russian Meteorology and Hydrology, 2013. vol. 38, no. 3, pp. 177-184 DOI: 10.3103/S1068373913030060.
12. Pustovalov K. N., Nagorskiy P. M., Oglezneva M. V, Smirnov S. V. Variability of the Integral Content of Dust Aerosol over Western Siberia and its Influence on the Surface Electric Field, Atmospheric and Oceanic Optics, 2024. vol. 37, no. S1, pp. S169-S174 DOI: 10.1134/S1024856024701562.

13. Karagioras A.,Kourtidis K. Study of the influence of local meteorology on the atmospheric potential gradient, Atmospheric Research, 2025. vol. 323, pp. 108168 DOI: 10.1016/j.atmosres.2025.108168.

14. James M. R., Lane S. J., Gilbert J. S Volcanic plume monitoring using atmospheric electrical potential gradiens, Journal of the Geological Society, 1998. vol. 155, no. 4, pp. 587-590 DOI: 10.1144/gsjgs.155.4.0587.

15. Morgunov V. A. Prostranstvennye neodnorodnosti elektricheskogo polya kak faktor lito-ionosfernykh svyazey / *Elektricheskoe vzaimodeystvie geosfernykh obolochek.* Moskva, OIFZ RAN, 2000, pp. 106-113 (In Russian).

16. Mather T. A., Harrison R. G. Electrification of volcanic plumes, Surveys in Geophysics, 2006. vol. 27, no. 4, pp. 387-432 DOI: 10.1007/s10712-006-9007-2.

17. Harrison R. G., Aplin K. L., Rycroft M. J. Atmospheric electricity coupling between earthquake regions and the ionosphere, Journal of Atmospheric and Solar-Terrestrial Physics, 2010. vol. 72, no. 5-6, pp. 376-381 DOI: 10.1016/j.jastp.2009.12.004.

18. Shevtsov B. M., Firstov P. P., Cherneva N. V., Holzworth R. H., Akbashev R. R. Lightning and electrical activity during the Shiveluch volcano eruption on 16 November 2014, tmospheric electricity coupling between earthquake regions and the ionosphere, 2016. vol. 16, pp. 871–874 DOI: 10.5194/nhessd-16-871-2016.

19. Firstov P. P., Akbashev R. R., Cherneva N. V., Shevtsov B. M., Holzworth R. H. Atmospheric electric effects during the explosion of Shiveluch volcano on November 16, 2014, Izvestiya, Atmospheric and Oceanic Physics, 2017. vol. 1653, no. 5-61, pp. 24-31 DOI: 10.1134/S0001433817010066.

20. Akbashev R. R., Malkin E. I., Cherneva N. V. Characteristic Electrostatic Structure of Eruptive Plumes Emitted by Large Explosive Eruptions of Shiveluch and Bezymyanniy Volcanoes, Kamchatka, Journal of Volcanology and Seismology, 2024. vol. 18, no. 4, pp. 323-339 DOI: 10.1134/S0742046324700672.

21. Corney R. C., Burns G. B., Michael K., Frank-Kamenetsky A. V., Troshichev O. A., Bering E. A., Papitashvili V. O., Breed A. M., Duldig M. L. The influence of polar-cap convection on the geoelectric field at Vostok, Antarctica, Journal of Atmospheric and Solar-Terrestrial Physics, 2003. vol. 65, no. 3, pp. 345-354 DOI: 10.1016/S1364-6826(02)00225-0.

22. Cherneva N. V., Firstov P. P. *Formation of the local electric field of the atmosphere in Kamchatka under the influence of natural processes.* Vladivostok: Dalnauka, 2018. 134 c.

23. Tacza J., Raulin, J. P., Macotela E., Marun A., Fernandez G., Bertoni F. C. P., Lima L. M., Samanes J., Buleje Y., Correia E., Alves G., Makita K. Local and global effects on the diurnal variation of the atmospheric electric field in South America by comparison with the Carnegie curve, Atmospheric Research, 2020. vol. 240, pp. 104938 DOI: 10.1016/j.atmosres.2020.104938.

24. Slyunyaev N. N., Sarafanov F. G., Ilin N. V., Mareev E. A., Volodin E. M., Frank-Kamenetsky A. V., Williams E. R. The Seasonal Variation of the Direct Current Global Electric Circuit: 1. A New Analysis Based on Long-Term Measurements in Antarctica, Journalof Geophysical Research: Atmospheres, 2025. vol. 130, no. 6 DOI: 10.1029/2024JD042633.

25. Sheftel V. M. Bandilet O. I., Yaroshenko A. N., Chernyshev A. K. Space-time structure and reasons of global, regional, and local variations of atmospheric electricity, Journalof Geophysical Research, 1994. vol. 99, no. D5, pp. 10797–10806 DOI: 10.1029/93JD02857.

26. Martell E. A. Enhanced ion production in convective storms by transpired radon isotopes and decay products, Journal of Geophysical Research, 1985. vol. 90, no. D4, pp. 5909-5916 DOI: 10.1029/JD090iD04p05909.

27. Firstov P. P., Cherneva N. V., Ponomarev E. A., Buzevich A. V. Podpochvennyy radon i napryazhennost' elektricheskogo polya atmosfery v rayone Petropavlovsk-Kamchatskogo geodinamicheskogo poligona [Subsoil radon and electric field intensity in the atmosphere in case of Petropavlovsk-Kamchatsky geodynamic chain in 1998-2003], Vestnik KRAUNTS. Ser. Nauki o Zemle., 2006. vol. 1, no. 7, pp. 102–109 (In Russian).

28. Petrov A. I., Petrova G. G., Panov V. M. Profiles of polar conductivities and of radon-222 concentration in the atmosphere by stable and labile stratification of surface layer, Atmospheric Research, 2009. vol. 91, no. 2-4, pp. 206–212 DOI: 10.1016/j.atmosres.2008.06.015.

29. Golubenko K., Rozanov E., Mironova I., Karagodin A., Usoskin I. Natural Sources of Ionization and Their Impact on Atmospheric Electricity, Geophysical Research Letters, 2020. vol. 47, no. 12, pp. e2020GL088619 DOI: 10.1029/2020GL088619.

30. Märcz F. Short – term changes in atmospheric electricity associated with Forbuch decreases, Journal of Atmospheric and Solar-Terrestrial Physics, 1997. vol. 59, no. 9, pp. 975-982 DOI: 10.1016/S1364-6826(96)00076-4.

31. Kuznetsov V. V., Cherneva N. V. Issledovaniye Forbush-ponizheniy i effektov terminalora v atmosfernom elektricheskom pole na observatorii "Paratunka" [Study of forbush decreases and terminator's effects in atmospheric electric field conducted at «Paratunka» observatory, Kamchatka], Vestnik KRAUNTS. Ser. Nauki o Zemle, 2008. vol. 1, no. 11, pp. 89–97 (In Russian).
32. Kleimenova N., Kozyreva O., Kubicki M., Michnowski S. Variations of the Mid-Latitude Atmospheric Electric Field (Ez) Associated with Geomagnetic Disturbances and Forbush Decreases of Cosmic Rays, JPublications of the Institute of Geophysics, Polish Academy of Sciences, Series M: Miscellanea, 2009. vol. D-73, no. 412, pp. 55-64.
33. Smirnov S. Fair Weather and Electric Field Convective Generator, Atmosphere, 2025. vol. 16, no. 11, pp. 1282 DOI: 10.3390/atmos16111282.
34. Kleimenova N., Kozyreva O., Michnowski S., Kubicki M. Influence of geomagnetic disturbances on atmospheric electric field (Ez) variations at high and middle latitudes, Journal of Atmospheric and Solar-Terrestrial Physics, 2013. vol. 99, pp. 117-122 DOI: 10.1016/j.jastp.2012.07.009.
35. Morozov V. N., Kupovykh G. V. *Mathematical modeling of the global atmospheric electrical circuit and surface layer electricity.* St. Petersburg: Asterion, 2017. 307 c.
36. Kasemir H. W. Theoretical Problems of the Global Atmospheric Electric Circuit / *Electrical Processes in Atmospheres. In: Dolezalek H., Reiter R., Landsberg H.E. (eds).* Darmstadt, Steinkopff, 1976, pp. 423-438.
37. Firstov P. P., Cherneva N. V., Buzevich A. V. [et al.] On the effects of air pressure variations on radon exhalation into the atmosphere, Journal of Volcanology and Seismology, 2007. vol. 1, no. 6, pp. 397-404 DOI: 10.1134/S0742046307060036.
38. Kasemir H. W. Zur Strömungstheorie des luftelektrischen Feldes III: Der Austauschgenerator, Archiv für Meteorologie, Geophysik und Bioklimatologie, 1956. vol. A, no. 9, pp. 357–370 DOI: 10.1007/BF02247454.
39. Park C. G. Downward mapping of high-latitude ionospheric electric fields to the ground, Journal of Geophysical Research, 1976. vol. 81, no. 1, pp. 168-174 DOI: 10.1029/JA081i001p00168.
40. Reiter R. Solar flares and their impact on potential gradient and air-earth current characteristics at high mountain stations, Pure and Applied Geophysics, 1966. vol. 72, no. 1, pp. 259-267 DOI: 10.1007/BF00875709.
41. Tinsley B. A., Yu F. Atmospheric Ionization and Clouds as Links Between Solar Activity and Climate / *Solar Variability and Its Effects on Climate. In J. M. Pap, P. Fox, C. Frohlich, H. S. Hudson, J. Kuhn, J. McCormack, G. North, W. Sprigg S. T. Wu (Eds.),*, 141. Washington, American Geophysical Union, 2004, pp. 321–339.
42. Druzhin G. I.,. Cherneva N. V, Melnikov A. N. Thunderstorm activity according to VLF observations at Kamchatka, Geomagnetism and Aeronomy, 2009. vol. 8149, no. 8, pp. 1305-1307 DOI: 10.1134/S001679320908057X.
43. Kuznetsov V. V., Cherneva N. V., Babakhanov I. Yu. Effect of an artificial cloud on the atmospheric electric field, Izvestiya, Atmospheric and Oceanic Physics, 2007. vol. 43, no. 2, pp. 237-242 DOI: 10.1134/S0001433807020107.
44. Cherneva N. V., Ponomarev E. A., Firstov P. P., Buzevich A. V. Bazovyye modeli istochnikov variatsiy vertikal'noy komponenty atmosfernogo elektricheskogo polya [BASIC MODELS OF SOURCES OF ATMOSPHERIC ELECTRIC FIELD VERTICAL COMPONENT VARIATIONS], Vestnik KRAUNTS. Ser. Nauki o Zemle, 2007. vol. 2, no. 10, pp. 60-64 (In Russian).
45. Kuznetsov V. V., Cherneva N. V., Babakhanov I. Yu. Experiments with the active impact of steam jet on atmospheric electric field, Izvestiya, Atmospheric and Oceanic Physics, 2009. vol. 45, no. 6, pp. 751-756 DOI: 10.1134/S0001433809060085.
46. Sorokin V. M., Chmyrev V. M., Yashchenko A. K. Electrodynamic model of the lower atmosphere and the ionosphere coupling, Journal of Atmospheric and Solar-Terrestrial Physics, 2001. vol. 63, no. 16, pp. 1681-1691 DOI: 10.1016/S1364-6826(01)00047-5.
47. Rulenko O.P., Tokarev P.I. Atmospheric-electric effects of Large Fissure Tolbachik Eruption in July-October 1975, Byulleten' vulkanologicheskikh stantsiy, 1979. vol. 56, pp. 96-102.
48. Behnke S. A., Thomas R. J., Krehbiel P. R., McNutt S. R. Spectacular lightning revealed in 2009 Mount Redoubt eruption, Eos, Transactions American Geophysical Union, 2012. vol. 93, no. 20, pp. 193-194 DOI: 10.1016/S1364-6826(96)00076-4.
49. Behnke S.A., Thomas R.J., McNutt S.R., Schneider D.J., Krehbiel P.R., Rison W., Edens H.E. Observations of volcanic lightning during the 2009 eruption of Redoubt Volcano, J Volcanol Geotherm Res, 2013. vol. 259, pp. 214–234 DOI: 10.1016/j.jvolgeores.2011.12.010.

50. Behnke S.A., McNutt S.R. Using lightning observations as a volcanic eruption monitoring tool, Bull Volcanol, 2014. vol. 76, no. 847 DOI: 10.1007/s00445-014-0847-1.
51. Firstov P.P., Malkin E.I., Akbashev R.R., Druzhin G.I., Cherneva N.V., Holzworth R.H., Uvarov V.N., Stasiy I.E. Registration of Atmospheric-Electric Effects from Volcanic Clouds on the Kamchatka Peninsula (Russia), Atmosphere, 2020. vol. 11, no. 643, pp. 1-16 DOI: 10.3390/atmos11060634.
52. Miura T., Koyaguchi T., Tanaka Y. Measurements of electric charge distribu-tion in volcanic plumes at Sakurajima Volcano, Japan, Bull. Volcanol, 2002. vol. 64, pp. 75–93 DOI: 10.1007/s00445-001-0182-1.
53. Antel C., Collier A. B., Lichtenberger J., Rodger C. J. Investigating Dunedin whistlers using volcanic lightning, Geophys. Res. Lett., 2014. vol. 41, pp. 4420–4426 DOI: 10.1002/2014GL060332.
54. Malkin E. I. et al. Remote methods for observations of Shiveluch and Bezymyanniy volcano eruptions, Vestnik KRAUNC. Fiz.-mat. nauki, 2023. vol. 43, no. 2, pp. 141-165 DOI: 10.26117/2079-6641-2023-43-2- 141-165.
55. Malkin E.I., Shevtsov B.M., Cherneva N.V., Kazakov E.A., Lichtenberger J. High-Altitude Discharges and Whistlers of Volcanic Thunderstorms, Atmosphere, 2024. vol. 15, no. 12, pp. 1503 DOI: 10.3390/atmos15121503.
56. Malkin E., Druzhin G., Firstov P., Cherneva N., Uvarov V., Sannikov D., Stasiy I. Principles of Creation of Local Network for Lightning Discharge Observations on Active Volcanoes of Kamchatka Peninsula / *E3S Web of Conferences*, Solar-Terrestrial Relations and Physics of Earthquake Precursors, vol. 127. France, EDP Sciences, 2019, pp. 02021 DOI: 10.1051/e3sconf/201912702021.
57. Malkin E., Cherneva N., Akbashev R., Sannikov D., Druzhin G. The Mechanism of Thunderstorm Formation in Eruptive Clouds on the Example of Bezymyanny Volcano Eruptions / *Springer Proceedings in Earth and Environmental Sciences*, Problems of Geocosmos–2022. In: Kosterov, A., Lyskova, E., Mironova, I., Apatenkov, S., Baranov, S. (eds), Springer, Cham., 2023 DOI: 10.1007/978-3-031-40728-4_33.
58. Mikhailov Y. M. *Low frequency electromagnetic waves: Space and ground experiments (Second edition)*. LAP: Lambert Academic Publishing, 2020. 100 pp.
59. Malkin E. I., Kazakov E. A., Sannikov D. V., Cherneva N. V., Marchenko L. S., Drugin G I. Statistical relationship between whistlers and sprites according to AWDANET and WWLLN data, Vestnik KRAUNC. Fiz.-mat. nauki, 2022. vol. 41, no. 4, pp. 178-190 DOI: 10.26117/2079-6641-2022-41-4-178-190.
60. Koronczay D.,. Lichtenberger J, Clilverd M. A. [et al.] The Source Regions of Whistlers, Journal of Geophysical Research: Space Physics, 2019. vol. 124, no. 7, pp. 5082-5096 DOI: 10.1029/2019JA026559.

Information about the authors

Malkin Evgeny Ilyich – Ph.D. (Phys. & Math.), Researcher at the Laboratory of Electromagnetic Radiation, Institute of Cosmophysical Research and Radio Wave Propagation, Far Eastern Branch of the Russian Academy of Sciences, Paratunka, Russia, ORCID 0000-0001-8037-1335.

Cherneva Nina Volodarovna – Ph.D. (Phys. & Math.), Leading Researcher at the Laboratory of Electromagnetic Radiation, Institute of Cosmophysical Research and Radio Wave Propagation FEB RAS, Paratunka, Russia, ORCID 0000-0002-6440-7569.